Erosion-driven vertical motions of the circum Arctic: Comparative analysis of modern topography

Sergei Medvedev[1,*], Ebbe H. Hartz[2,1], Jan Inge Faleide[1]

1 Centre for Earth Evolution and Dynamics (CEED), University of Oslo, Oslo, Norway

2 AkerBP ASA, Lysaker, Norway

* Corresponding author, e-mail sergei.medvedev@geo.uio.no

Abstract

Deep and complex geodynamic processes, including the effects of plumes, heat, plate tectonics, and local tectonics control the Earth's surface. In the Arctic these deep processes are masked by extensive glaciations and associated or roughly synchronous erosion. In this study we aim to reveal these hidden geodynamic processes by modeling erosion backward in time by numerically restoring eroded material and calculating the flexural isostatic response repeatedly iteratively until eroded features are filled. This method estimates erosion recorded in the modern topography and models the influence of that erosion. Although the obvious topographic response to erosion is a lowering of the elevation, our coupled erosion-isostatic response method results in dramatic vertical motions leading to km-scale uplift in fjord carved areas of Scandinavia, Greenland, and Canadian Arctic Archipelago and supporting ancient orogenic belts of northern Siberia and northern Alaska to stay at high elevation. Sensitivity testing confirms the utility of our method over a range of effective elastic plate thicknesses as well as for laterally varying elastic thickness. Comparison of modelling results with observed gravity anomalies shows that our method is valid for both glacial and fluvial affected landscapes but more importantly links surface and deep Earth dynamics. Combined analysis of the gravity anomalies and model results also explains erosion as one of the main mechanisms responsible for gravity signal for tectonically inactive regions and illustrates the interaction of short wavelength erosional processes and large scale, regional processes like active orogenesis and dynamic topography.

Keywords: Arctic, erosion, isostasy, numerical modelling

1. Introduction

Prompted by recent climate change, as well as political and economic motives, interest for studying the Arctic has increased in the last decade. Several international efforts have contributed to large, regional data compilations revealing a much more complicated structure of the Arctic crust than previously thought (e.g., Gaina et al., 2014; Harrison et al., 2011; Pease et al., 2014; Petrov et al., 2016).

In short, the Arctic displays remnants of old orogenic belts such as the Caledonides, the Verkhoyansk-Chersky orogeny in Siberia, and the Urals, all formed during the amalgamation of Pangea (Torsvik and Cocks, 2016; Veevers, 2004). The now-Arctic region of the supercontinent experienced major volcanic events, most notably the Permo-Triassic Siberian Traps and Cretaceous High Arctic large igneous province (Buchan and Ernst, 2006; Gaina et al., 2014), before breaking up into the continents we know today. The break up was preceded by long periods of continental extension. In the Arctic, break up initiated in the Cretaceous. The Canada Basin, most likely, developed as a rotational opening between Alaska-Western Russia and northern Canada (Grantz et al., 2011). Roughly synchronous with the early extension and break up of Pangea, collisional orogens began to form in Eastern Siberia and Alaska.

The final break up of Pangea occurred by the northwards propagation of the Atlantic rift into the northwestern and northeastern Atlantic and the Eurasia Basin (see e.g. Torsvik et al., 2002 for review). During this final break up, active magmatism affected Greenland and subsequently the northeast Atlantic (Gaina et al., 2014; Lawver and Muller, 1994). In addition to these tectonic and volcanic events,

vertical motions, with less obvious and probably deep seated origin, have influenced the region (Japsen and Chalmers, 2000). Parallel to the formation of the North Atlantic Ocean a huge orogenic belt began to rise in Alaska where the Pacific and North American Plate converge (Fitzgerald et al., 1993).

All of these events left a persistent imprint on the rocks and landscapes of the region, and they are all much debated in the literature, both from an observational and modelling perspective (Miller et al., 2018). In contrast, the effects of the Late Cenozoic, mostly glacial, erosion of the Arctic as a whole are rarely discussed, despite their obvious influence on shaping the Arctic as we know it today (Figure 1 and Figure 2).

The Arctic region, especially areas around North Atlantic and the circum Greenland realm, is characterized by dramatic landscapes with major fjord inlets and associated deltas with erosional products (Figure 1 and Figure 2). These processes caused substantial redistribution of mass, which loaded the lithosphere where sediment accumulated and unloaded in eroded areas. An associated enigma is that these heavily eroded areas are also characterized by remnants of large marine sedimentary basins uplifted high above sea level without an obvious tectonic cause.

Collectively, these morphological and geological observations have motivated us to analyze the influence of erosion on vertical movements of the Arctic lithosphere. We modelled the entire circum Arctic within a single model to compare amplitudes of effects. The study does not try to construct precise maps of erosional effects, but to distinguish regions were erosion effects are well pronounced and to roughly estimate these effects. A similar approach was demonstrated in Medvedev et al. (2013), whereas more detailed and accurate analysis may be provided within more regional studies (e.g., Champagnac et al., 2007; Medvedev et al., 2008; Steer et al., 2012).

We use a numerical technique *Erosion Backward in Time* (EBT), which has already been applied successfully to regional studies. Ice-related erosion partially explains the enigmatic uplift of Mesozoic marine sediments along passive margins of eastern Greenland (Medvedev et al., 2008; Medvedev et al., 2013) and the evolution of paleo-plateaus in western Greenland (Medvedev et al., 2013). Applied to Scandinavia (Medvedev and Hartz, 2015), EBT not only restores the pre-erosional landscape, but also explains features of long-term evolution of Scandinavian topography using the distribution of fission track ages.

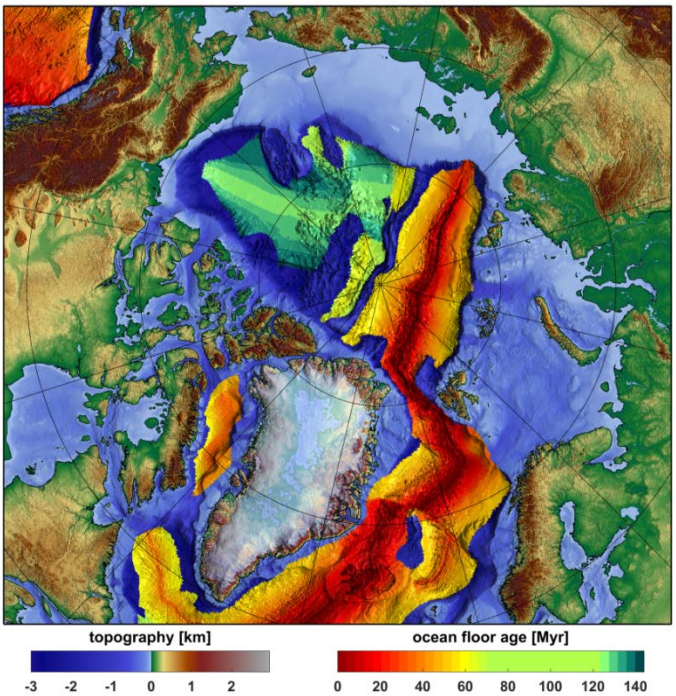

Figure 1. Study area: topography of the continental part (updated 15" version of Becker et al., 2009) and age of the ocean floor (Gaina et al., 2017; Muller et al., 2008). Thickness of Greenland ice cap from Amante and Eakins (2009).

Figure 2. The inner Hardangerfjord of southwestern Norway is a typical example of an ice-carved fjord, which cut ca. 2 km into a paleic surface. The fjord in foreground is ca. 3 km wide).

2. Numerical models using Erosion Backward in Time (EBT)

2.1. Modelling approach

The primary target of this research is to analyze of the effect of unloading the continental part of the Arctic realm by erosion. Our study does not consider physical mechanisms of erosional process, but rather estimates the effect of erosion on the topography, lithosphere, and vertical motions by quantifying (1) the amount of erosion as evidenced by modern topography, and (2) vertical motions of the lithosphere caused by unloading the eroded material.

By analyzing only erosional unloading, we ignore the second part of erosional mass redistribution, which is the accumulation of sediments and corresponding loading of the lithosphere. A lack of detailed data in most of the Arctic precludes us from studying sediment accumulation. However, we estimate the potential interference of sediment loading on our results using a regional example (Appendix B; see location of example in Figure 3). That example shows limited effect of off-shore sedimentation and that allows us to consider erosional unloading separately in our globally-oriented study.

Our previous studies use EBT by filling concave shapes to reconstruct pre-erosional topography assuming that there was some form of “old” paleic surface that was carved by erosion (Medvedev and Hartz, 2015; Medvedev et al., 2008; Medvedev et al., 2013). A typical example of such evolution can be development of fjords (e.g., in western Norway, Figure 2). EBT is not limited to studying glacial erosion only, although the method indeed predicts more pronounced effects when applied to localized carving by fjords. The purely geometrical approach of EBT, in fact, precludes it from recognizing the type of erosion and it can analyze any type of eroded topography that is characterized by an abundance of concavities.

The paradigm of erosion as localized carving of paleic surfaces is questioned even for the Arctic realm. Recent studies suggest considerable syn-glacial erosion of upper relatively flat surfaces (Andersen et al., 2016; Egholm et al., 2017; Nielsen et al., 2009; Steer et al., 2012). Many deeply eroded regions are represented by terrains dominated by peaks rather than flat-topped mountains (e.g., Denali in central Alaska; Fitzgerald et al., 1993). Outside areas of major glaciation (e.g., Peltier, 2004), or in areas of past or ongoing tectonism, EBT requires different thinking. Some questions to consider are: Was there an initial paleic surface? What was the timing of erosion? Can concave shapes in the topography be locations of orogenic synclines or footwalls of thrusts, rather than just the result of erosion? Without possibility to fully resolve these enigmas, we apply EBT to all types of landscapes (incised by fluvial,

glacial, and/or combined types of erosion) to understand the way of estimating the erosion from modern topography.

In the case of absence of a paleic surface, we use EBT to fill the modern topography, realizing that the resulting surface may never have been an actual surface. Thus we need to understand what is meant by the modelled "pre-erosional topography." Backward in time modelling always results in losing the high-frequency signal, and thus the result of EBT cannot be a rough surface. Appendix A1 shows that if bulk volume of eroded material is known, the EBT pre-erosional topography adequately approximates pre-existing topography, even if it is a fluvial landscape. In the global approach of this study, the erosional mass balance cannot be accurately tested, and the pre-erosional topography can be considered as an enveloping surface of modern topography (Appendix A2). This approach does not mean to reconstruct real ancient topography, but allows estimation of erosion recorded within modern topography. This application ignores erosion of the modern peaks and flat surfaces and thus may be considered as conservative. In contrast, it may overestimate erosion of the orogenically controlled landscapes. These uncertainties do not significantly affect the results of this study, but should be considered carefully in regional applications.

2.2. Model set up

Figure 1 presents the geographical location and areas subjected to the model. Similar to Medvedev et al. (2013), calculations are performed on two grids. The topographic update model used a grid of about 3800 by 3600 grid cells, with ca. 1.5 km grid spacing. This part of model iteratively fills concave shapes on continental parts of the domain not covered by permanent ice caps (Figure 3, Appendix A). The continent-ocean boundary is mainly located at 800 to 1000 m water depth, the depth beyond which ice sheets are considered as impossible (Auriac et al., 2016; Patton et al., 2015). We also excluded the internally drained inner part of Greenland. The isostatic calculations assume a shear deformable elastic plate (Brush and Almroth, 1975; Kwon and Bang, 2000; Medvedev, 2016) and use a grid six times coarser than the topographic grid in both directions (9x9 km). The pure elastic model of the lithosphere assumes instantaneous reaction to the added load and thus time is not a parameter of the model. The lateral boundaries of the model domain are free to slip.

The main source of deformation in our model is topographic relief, thus we use the highest quality possible DEM such as the SRTM15+ (updated 15" version of Becker et al., 2009). The other model parameters were chosen to keep the model as simple as possible. Three main numerical parameters are the density of mantle (3300 kg/m^3 was used); density of eroded rocks (uniform values in the range of 2500 to 2800 kg/m^3 were tested); and effective elastic thickness of the lithosphere (EET, uniform and variable values in the range of 5 to 50 km were tested). The results presented below are mainly based on the model EET40 (uniform EET=40 km).

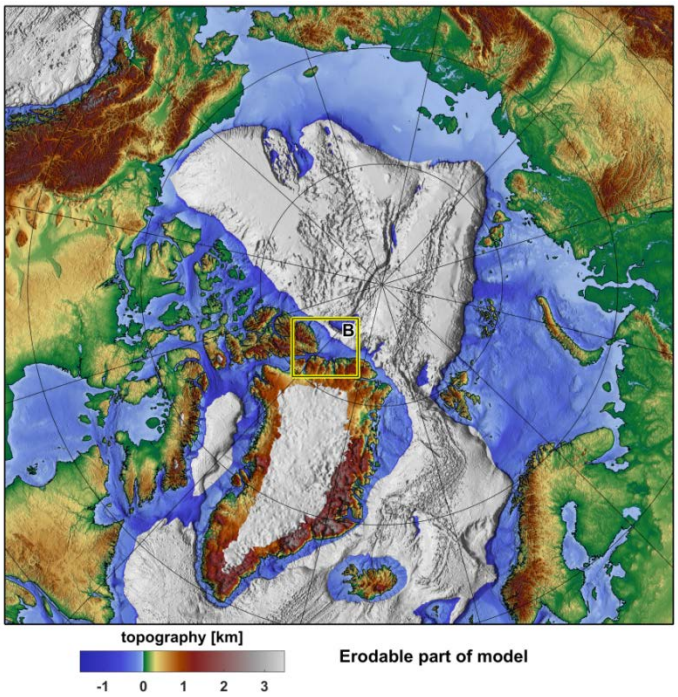

Figure 3. The area subjected to erosional processes within EBT is colored. The grey areas are either oceanic (see Fig. 1) or internally drained inner part of ice-covered Greenland. Box indicates location for study of sediment loading (Appendix B). .

2.3. General results of modelling

The erosion backward in time model (EBT) fills concave shapes with "placed-in" material(corresponds to "amount of erosion" if looking forward in time) and the final result is presented in Figure 4a. The erosional unloading results in lithospheric uplift forced by isostatic readjustment. In areas with extreme erosion (up to 3 km), such as East and West central Greenland and the Canadian Arctic Archipelago, lithospheric uplift exceeds 1 km (Figure 4b). Comparison of the localized erosion (Figure 4a) with the isostatic response smoothed by the flexurally strong lithosphere (Figure 4b) illustrates the cause of uplift of non-eroded areas adjacent to deeply eroded fjords even though, on average, the area subjected to erosion should subside.

Smooth pre-erosional topography (Figure 4c), where most of the fjords and valleys are filled to their summits, is the target result of EBT. The relief of the oceanic part remains unchanged (see Figure 3). The topography of the inner part of Greenland was also not subjected to EBT, but the ice cap was removed and the surface was readjusted isostatically (up to 800 m; Medvedev et al., 2013). In general, the overall topography subjected to EBT became flatter, with peaks lowered and depressions elevated. Some islands in the western part of the Canadian Arctic Archipelago lie below sea level and their rise above sea level is caused by active erosion of the surrounding areas (outlined by white in Figure 4c, see also section 3.1). The amplitude of surface processes, lithospheric response, and, particularly, uplift of Arctic islands is larger than prior estimates estimated for Greenland (Medvedev et al., 2013) and for Scandinavia (Medvedev and Hartz, 2015).

Large amplitude effects in Alaska and north central Siberia (upper part in Figure 4) reflect an extreme topographic relief caused by a mixture of orogenic processes and erosion, both glacial and fluvial, whereof some probably pre-date the Quaternary glaciations. These mechanisms cannot be distinguished by our simple model, which assumes that all topographic concavities are erosional, so in these regions the calculated erosion may include tectonic components.

2.4. Topography changes during erosion

Large amplitude surface processes and isostatic readjustments change topography significantly (cf. Figure 1 and Figure 4). The natural topographic response to erosion is the lowering of topography in

the eroded areas. The combination of erosion and elastic isostatic response, however, results in major topographic uplift in several locations (Figure 5). Some of these areas, where uplift occurs rather than expected subsidence, are clearly related to glacial erosion. The most striking effect is the uplift of the Arctic Canadian Archipelago (area 1 in Figure 5), the islands of the Barents and Kara seas (Figure 5), and areas around the large fjords of the central Greenland, along the east and west coast (area 4; also described in Medvedev et al., 2013). Alaska (area 2) and the Verkhoyansk area in Siberia (area 3 in Figure 5) demonstrate large amplitude topography changes, although the erosional pattern of these areas is not as strongly localized as the areas of the bottom part of Figure 5 and is not dominated by fjord incisions.

In contrast to the areas discussed above, the Barents Shelf and Kara Sea (Figure 5) are submerged below sea level. The modern bathymetry of the seas shows the clear influence of glacial erosion in the form of underwater channels, which can be as much as 300 m deeper than the average seafloor. These channels may be considered as underwater fjords and, similar to fjords, uplift surrounding areas when eroded. For example, about 500 m uplift of Novaya Zemlya was caused by the erosion of adjacent channels offshore (see blue stripes along shores of Novaya Zemlya in Figure 5). Development of "traditional fjords" of Svalbard resulted in the uplift of parts of the island by 300-400 m.

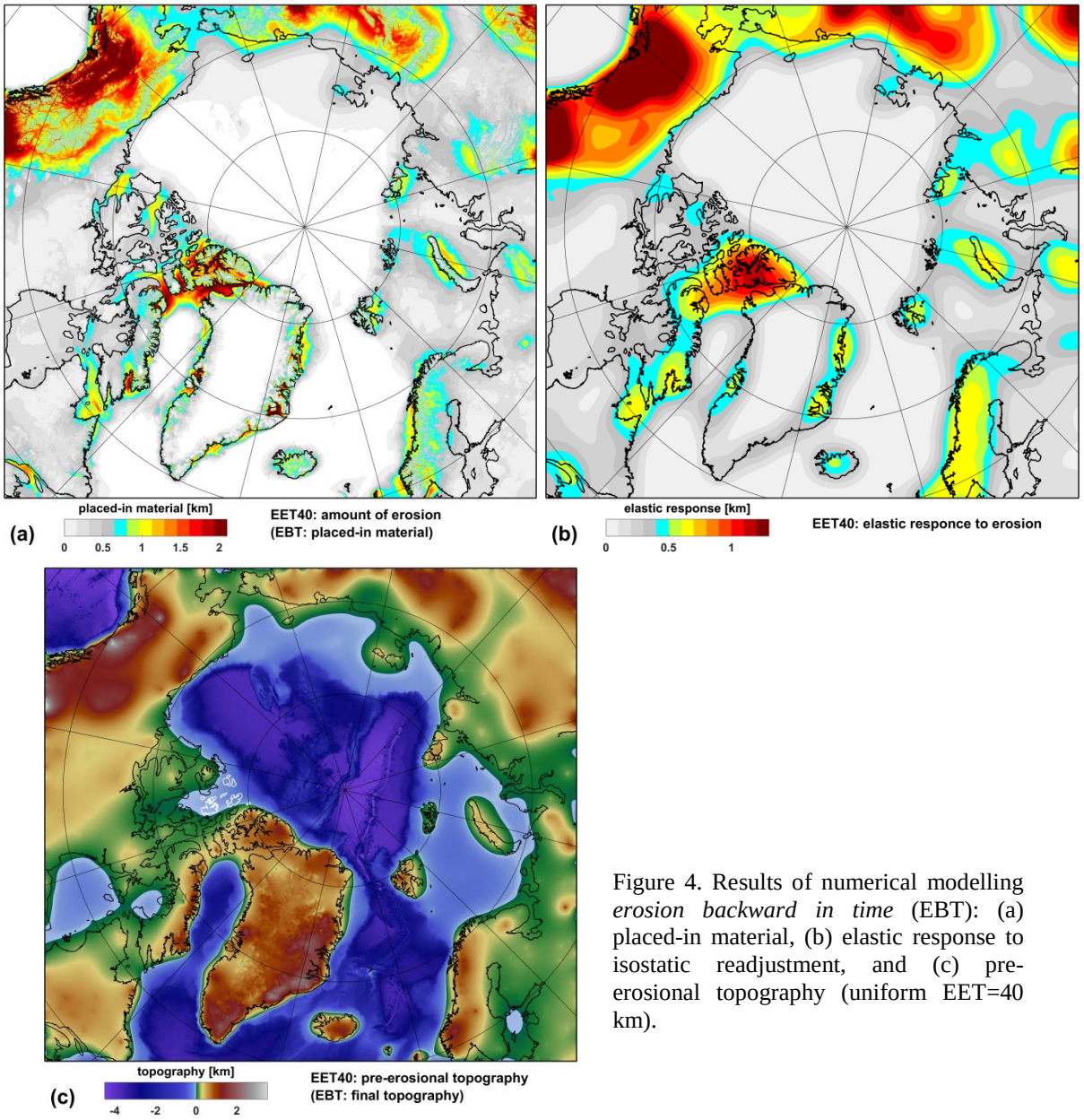

Figure 4. Results of numerical modelling *erosion backward in time* (EBT): (a) placed-in material, (b) elastic response to isostatic readjustment, and (c) pre-erosional topography (uniform EET=40 km).

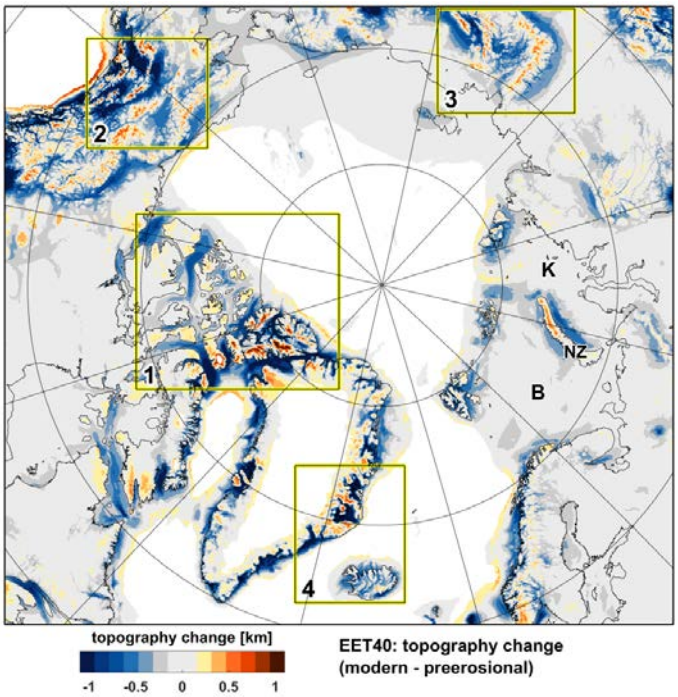

Figure 5. Topography change: modern topography minus pre-erosional topography. Orange to red colors indicate significant uplift caused by erosion. The boxes outline areas of regional studies, 1 – 3 in section 3 and 1 – 4 in section 4. B = Barents Sea, NZ = Novaya Zemlya, K = Kara Sea.

2.5. Model restrictions and parameter check

The Arctic is characterized by a series of major offshore sedimentary basins, many of which are related to Quaternary glacial erosion (e.g., deltas along eastern and northern edges of the Barents Sea and along the northern edge of Canadian Arctic Archipelago). Our numerical treatment, however, ignores the process of sediment accumulation because the data on sediment structure is unavailable for a major portion of the study area. Appendix B analyzes a sedimentary basin in the Lincoln Sea and demonstrates that the offshore sediment accumulation may result in 200-300 m lithosphere subsidence within 100 km of adjacent coastal areas and insignificantly less subsidence further inland. Similar amplitudes were calculated for the sedimentary deltas along the western border of the Barents shelf. From the other hand, our pre-erosional topography often goes beyond shoreline (Figure 4). Thus, the main correction to the pre-erosional topography model may be overestimation of the coastal uplift and the sea-ward propagation of the shoreline should be smaller (as mentioned also in Steer et al., 2012).

Medvedev and Hartz (2015) demonstrated that variations in the strength of the lithosphere do not have major effects on topographic evolution modelled by EBT. The strength of the lithosphere, defined in our study by its Effective Elastic Thickness (EET), may vary significantly; this is caused by a number of modern and ancient reasons (e.g., Gac et al., 2016; Struijk et al., 2016). Appendix C tests the rheological dependence of our results with two series of experiments. In the first series, we compare two models with a different EET, one which is uniform across the model and one that tests the influence of lateral variations of EET. The results illustrate that amplitudes of effects are larger for areas with smaller EET, whereas the lateral extent of effects is wider for larger EET. Although these may be considered to be second order effects, the comparison of length scales of the erosion pattern and gravity signal (section 4) set preference of EET=40 km instead of 20 km for the base model presented in our study.

Our reference model, EET40, utilizes 2800 kg/m^{3}the as the density of the eroded material, which may be an acceptable density for upper crustal rocks. However, some areas, like the Sverdrup Basin in the Canadian Arctic Archipelago (section 3.1; Harrison et al., 2011) are dominated by sedimentary rocks and the density of the reference model thus may be too high. To analyze the degree that sediment density influences model results, we consider a model that utilizes a reduced density of 2500 kg/m^3. The

comparison for the area 1 (Figure 5) shows that the difference in pre-erosional topography, elastic response, and in amount of erosion is less than 160 m. This difference accounts for 10% of total effects and thus may be considered as a second order effect. However, the density of sediments in Sverdrup or other basins may be smaller than 2500 kg/m^3, and the effect may be larger.

3. Regional studies

Large vertical movements (Figure 4b) and/or large topographic changes observed in the circum-Arctic calculation (Figure 5) inspired us to examine several smaller regions for more detailed analysis (regions 1, 2, 3 in Figure 5). Some regions of high amplitude were already discussed in our previous studies, such as Greenland (Medvedev et al., 2008; Medvedev et al., 2013) and Scandinavia (Medvedev and Hartz, 2015). The amount of information available for the Barents-Kara seas region, including models of the lithosphere structure and thermal state (Gac et al., 2016; Klitzke et al., 2015; Klitzke et al., 2016; Minakov et al., 2012), data from seismic and well studies (Baig et al., 2016; Sobolev, 2012), and general compilations (Henriksen et al., 2011; Zattin et al., 2016) allows a more detailed analysis of this region and thus deserve a separate study.

3.1. Canadian Arctic Archipelago

The Canadian Arctic Archipelago, especially the large system of fjords of Ellesmere Island, is one of the key targets of our study. The effects of erosion are stronger here than in other parts of the Arctic (e.g., Medvedev et al., 2013). Moreover, the tectonic relationship between Greenland and Ellesmere Island has been subjected to long-standing debate (Cocks and Torsvik, 2011; Dawes, 2009; Torsvik et al., 2012). Regardless of plate configuration, it is clear that northwestern Greenland and Ellesmere Island experienced significant shortening and likely mountain building during the Eurekan orogeny (Piepjohn et al., 2016). This was caused by the Early to Mid-Cenozoic opening of the Labrador Sea and Baffin Bay and related compression north of Baffin Bay (Piepjohn et al., 2016)

The modern topography of the Canadian Arctic Archipelago is visibly dominated by major glacial carving between islands (Figure 6a). EBT estimates more than 2 km of eroded material (Figure 6b) and, consequently, more than 1.2 km of isostatic uplift (results in Figure 6c are presented for EET=40km, smaller EET results in much larger, up to 1.8 km for EET=20 km). The pre-erosional topography (Figure 6d) is smooth and, in general, not as high as modern islands; in fact, some islands do not even exist before glacial erosion, according to the model (e.g., Ellef Ringnes, Mackenzie King, and Bathurst, marked in Figure 6d). The EBT model thereby suggests a late Cenozoic uplift of the Late Paleozoic to Early Cenozoic marine deposits of the Sverdrup Basin in addition to active vertical motions during the Eurekan orogeny in early Cenozoic. The maps of topography changes (Figure 6e and f) indicate significant effects of erosion. Barbeau Peak, the tallest Canadian Arctic Archipelago mountain at 2616 m, indicates more than 800 m of erosional uplift in our model.

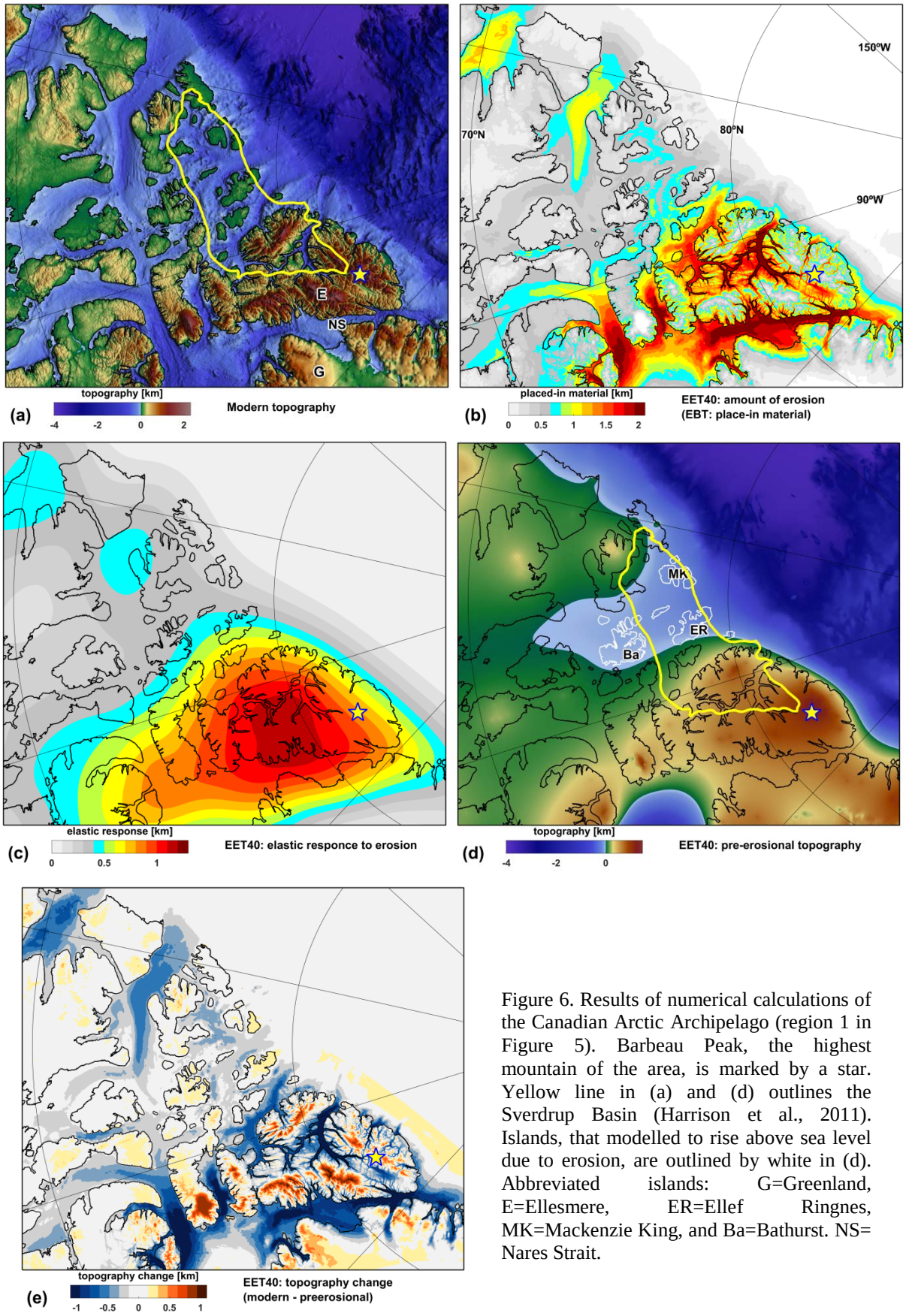

Figure 6. Results of numerical calculations of the Canadian Arctic Archipelago (region 1 in Figure 5). Barbeau Peak, the highest mountain of the area, is marked by a star. Yellow line in (a) and (d) outlines the Sverdrup Basin (Harrison et al., 2011). Islands, that modelled to rise above sea level due to erosion, are outlined by white in (d). Abbreviated islands: G=Greenland, E=Ellesmere, ER=Ellef Ringnes, MK=Mackenzie King, and Ba=Bathurst. NS= Nares Strait.

3.2. Circum Arctic orogenic belts

The previous applications of EBT assume that the topography is passively eroded from a paleic surface by glacial carving in the Quaternary. Outside areas of major glaciation (e.g., Peltier, 2004), or in areas of ongoing tectonism, EBT requires different thinking. That was the reason for introducing the generalized term of pre-erosional topography, the main target of EBT in Section 2.1 and Appendix A1 as a measure of erosion recorded in the modern topography, so as not to imply that the pre-erosional surface really existed. Arctic-wide analysis (Figure 5) proposes two regions: (a) Alaska, with its ongoing orogenesis, and (b) the deeply eroded remnant of the Verkhoyansk-Chersky orogen in north-central Siberia (regions 2 and 3 in Figure 5).

Alaska is characterized by active tectonics with active subduction along its southern coast (Fitzgerald et al., 1993; see also seismicity pattern in Fig. 7a), and progressively older mountain belts to the north (Figure 7, Coastal, Alaska, Yukon-Tanana Upland, and Brooks Range) separated by major sedimentary basins (Coney et al., 1980; Fuis et al., 2008). Central Alaska has few alpine glaciers today, it was not covered by major ice sheets during the last ice ages (Peltier, 2004), and the area was not deformed by major ice-streams as in Norway, the Canadian Arctic Archipelago, and Greenland. However, the resulting magnitude of erosion is at least as strong, and thus erosion must be in part older than recent glaciations elsewhere and mainly fluvial in nature.

EBT applied to this region results in some of the most extreme values we have calculated, up to 3.3 km erosion and more than 2 km elastic response (Figure 7b and c). The combination of major mountain ranges and intervening basins causes EBT to produce up to 2 km topographic changes in both vertical directions, up and down. EBT calculates that if Mount Denali (6190 m) was sculpted by erosional processes, it would be uplifted by 2.2 km (Figure 7c). It is important to remember that our calculation does not consider the particular mechanism of erosion (fluvial or glacial), nor the tectonic activity of the region (Eberhart-Phillips et al., 2003). Fitzgerald et al. (1993) estimated the uplift of Denali as 6 km during the last 6 Myr, 3.7 km of which was claimed to be tectonically induced. The remaining 2.3 km was attributed to isostatic rebound caused by exhumation, which compares well with 2.2 km estimated by our model.

Similar to Alaska, area 3 (Figure 5) in north central Siberia is dominated by a prominent mountain belt, but in this case the Verkhoyansk and Chersky mountains represent remnants of a Late Jurassic to Early Cretaceous orogeny (Figure 8; Prokopiev, 2000). Recent seismic activity in the region probably reflects adjustments along the triple junction between the Eurasian, North American, and Sea of Okhotsk plates (Parfenov et al., 1988). These old mountain belts (Figure 8) are deeply eroded by an erosional system that includes the Lena, Yana, and Indigirka rivers. The modern tectonic activity in the region is not as impressive , but the effects predicted by EBT in northern Siberia are almost as pronounced as those in the Alaska region (Figure 8), which may reflect longer lasting erosion.

The observations of this section allow us to speculate, comparing the styles of topography and modelled erosion for the Arctic. A first order observation is that the ice-carved systems of, for example, Greenland and Northeastern Canada (Figure 6), display less erosional effects than the less glaciated mountain belts of Alaska and Siberia (Figure 7 and Figure 8). Secondly, we note that although these mountains have been glaciated in the past and in part still are, their dominant erosion mechanism appears to be fluvial, evidenced from the existence of the major rivers and absence of major fjords in the region and on the modelled erosional pattern, which is less localized than in glacial-dominated areas (cf. Figure 7b and Figure 8b with Figure 6b). These two observations demonstrate that rivers are at least as active an erosion agent as glaciers, as proposed by Koppes and Montgomery (2009).

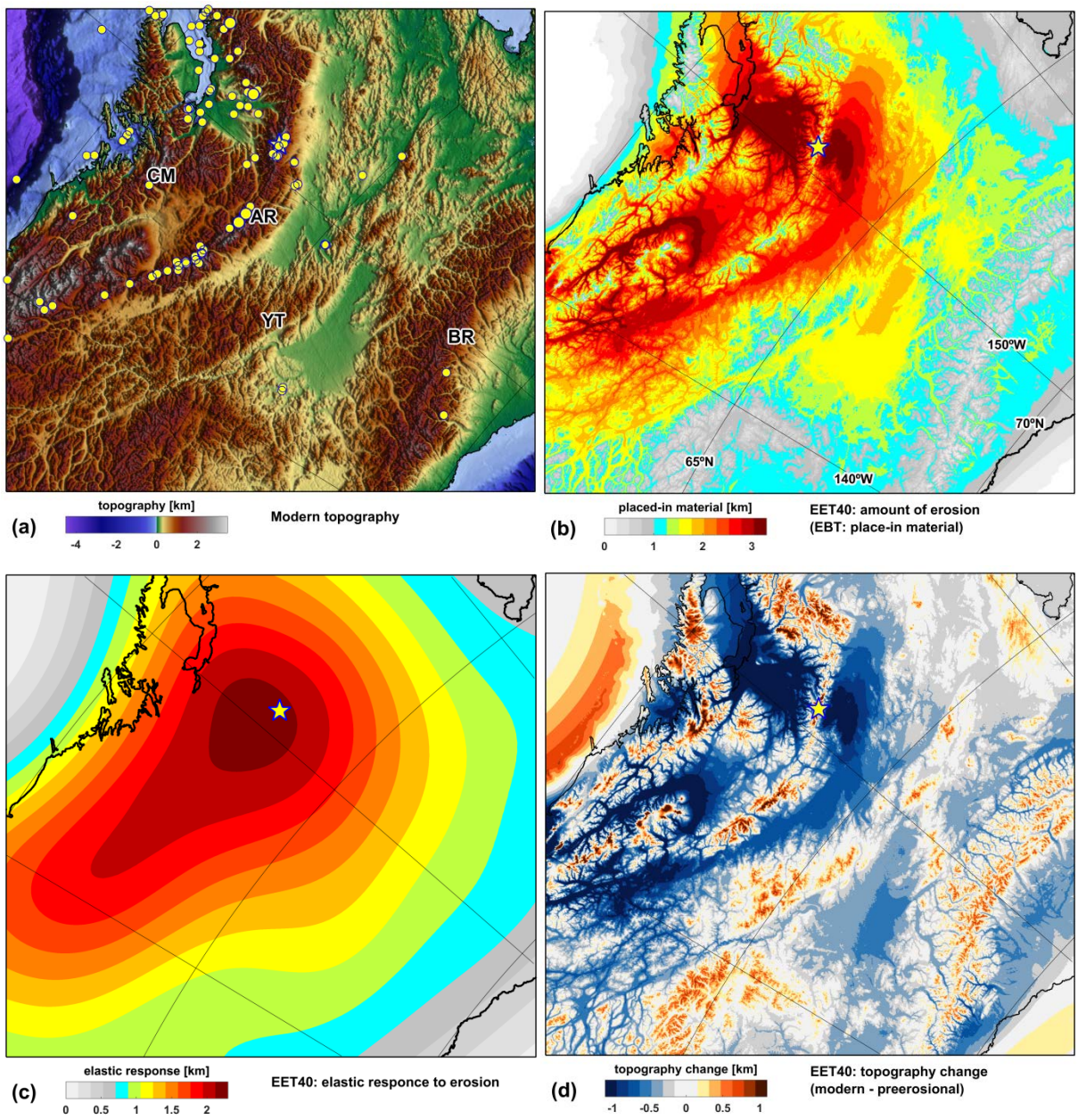

Figure 7. Modern topography and results of EBT in Alaska (region 2 in Figure 5). Star indicates the location of Mount Denali (6190 m). Yellow circles in (a) show locations of magnitude 5+ earthquakes during last 20 years (USGS Earthquake Catalog, earthquake.usgs.gov). Note that color scales in (b) and (c) differ from other figures. CM=Coast Mountains, AR=Alaska Range, YT=Yukon-Tanana Upland, BR=Brooks Range.

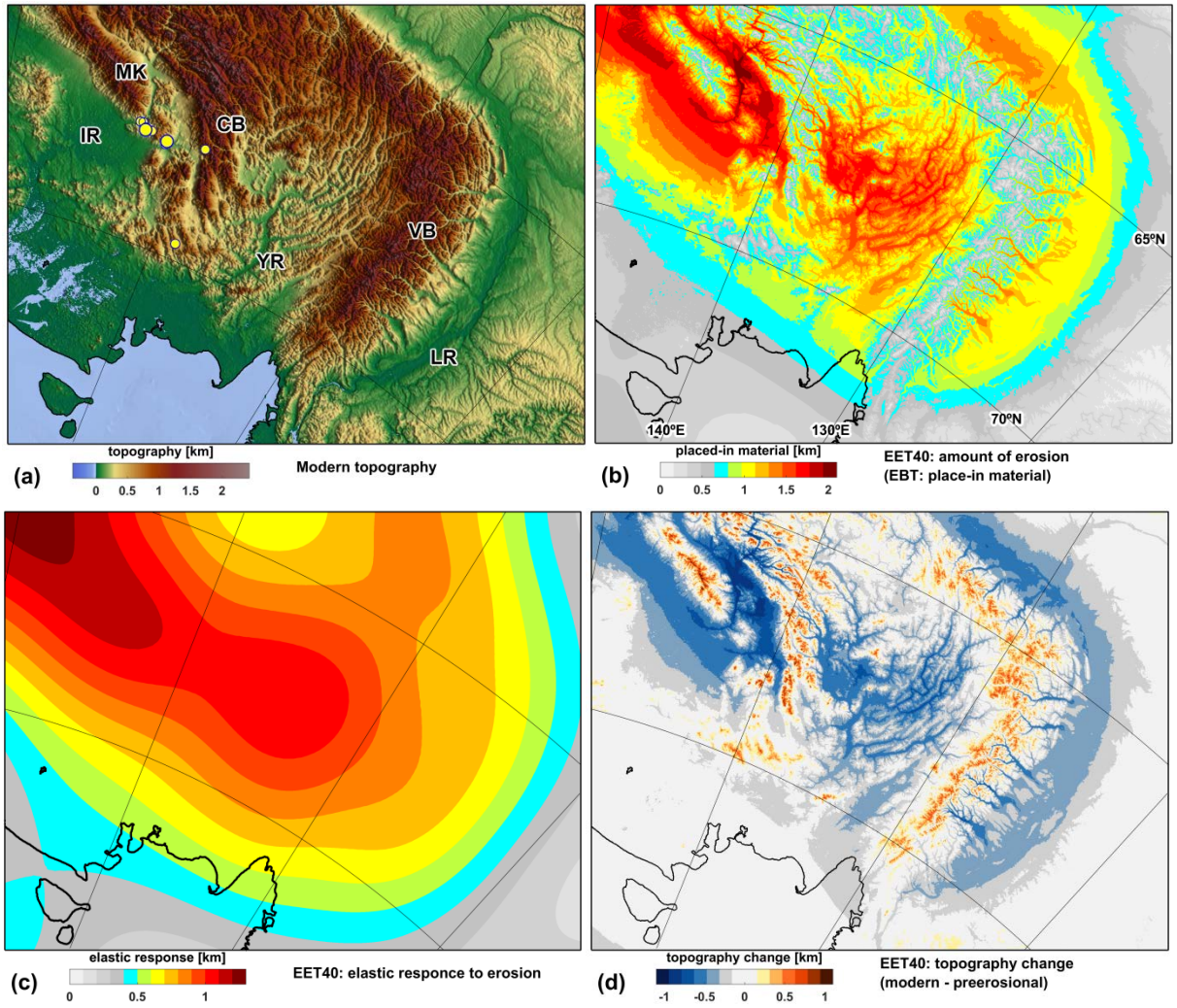

Figure 8. Modern topography and results of EBT in in north central Siberia (region 3 in Figure 5). Yellow circles in (a) show location of magnitude 5+ earthquakes during last 20 years (USGS Earthquake Catalog). IR=Indigirka River, YR=Yana River, LR=Lena River, VB=Verkhoyansk Belt, CB=Chersky Belt, MK=Momskiy Khrebet.

4. Comparison of model results with gravity anomalies

The modelled erosion (Fig. 4a and panels b in Figs. 6–8) indicates masses of material which left the system from the surface, whereas isostatic uplift (Fig. 4b and panels c in Figs. 6–8) indicates income of the mantle material into the system from beneath. These mass redistributions, localized for erosion and smooth for flexural isostasy, result in local mass excess or deficit. Figure 9a and Figure 10b present this mass (per unit area) misbalance ΔM measured in thickness of excess mantle material Δh and calculated acknowledging density difference between eroded, ρ_e, and mantle, ρ_m, materials.

$$\Delta M = \rho_m \Delta h = \rho_m h_m - \rho_e h_e \quad (1)$$

where h_e is thickness of eroded material and h_m is amount of lithospheric uplift, equal to influx of the mantle material (Figure 10b). Our model assumes isostatic readjustment of redistribution of material in the system such that ΔM is zero over large area. If we assume local (Airy) isostasy for pre-erosional configuration, the combination of localized erosional unloading and isostatic readjustment smoothed by the lithosphere should result in local isostatic disequilibrium or $\Delta M \neq 0$. This disequilibrium, in turn, results in gravity anomalies (Fowler, 1990), which can be approximated by (Turcotte and Schubert, 2002):

$$\Delta g = 2\pi G \Delta M = 2\pi G \rho_m \Delta h \quad (2)$$

where G is the gravitational constant. Eq. (2) results in about 140 mGal of gravity anomaly per each km of excess mantle material (see also Molnar et al., 2015).

Using equation (2), we compare results of the model Δg_{EET40} with observed free-air gravity anomaly Γ (Figure 9b). Difference of these two fields, $\Gamma - \Delta g_{EET40}$ (Figure 9c), demonstrates significant decrease in amplitude of anomalies (cf. Figure 9b) and thus illustrates that modelled erosion accounts for most of the gravity signal. That is even more evident from the high correlation of model and gravity observation along a profile (Figure 10c, note that modelled by EBT signal was smoothed to match resolution of gravity measurements).

Iceland and eastern Greenland, in contrast, shows opposite correlation and thus, a correction for erosion only amplifies the gravity signal (cf. Figure 11 a and b). This amplification, however, displays a positive regional trend. The area is known to have strong positive dynamic topography associated with large-scale positive buoyancy anomaly in the mantle under Iceland (Conrad et al., 2004; Flament et al., 2013). Schiffer and Nielsen (2016) estimated the regional dynamic uplift in the region in the range of 300-700 m, which would result in a regional gravity anomaly of 40-100 mGal (eq. 2). Subtracting 40 mGal from the observed gravity results in a strong correlation with the erosion-induced gravity signal (Figure 11c). Thus we suggest that the gravity anomaly signal in this region is dominated by two main effects, dynamic topography and erosion. This analysis also brings additional support to the estimations of dynamic topography amplitude of Schiffer and Nielsen (2016). Similar analysis of separation of regional and local scales gravity signal was applied to the Svalbard region in Minakov (2018).

Large amplitude of modelled erosion in areas dominated by orogenic landscapes (Figs. 7 and 8) corresponds to large amplitude of gravity anomalies (Figure 12a and Figure 13a). A direct correlation between observed gravity and erosion-induced gravity signal, however, is not straightforward. The top-left part on the area maps of amplitude changes (Figure 12b and Figure 13b) shows both strong correlation and strong anti-correlation. These areas can be associated with present day tectonic activities in Coast Mountains and Alaska Range in Alaska and Chersky Belt and Momskiy Khrebet in Siberia as indicated by earthquake distribution (Figure 12a and Figure 13a). Thus, the gravity signal is less controlled by erosion in these areas. This is also visible on the left part of profiles across the areas (Figure 12c and Figure 13c). The right-bottom parts of the chosen areas and right part of profiles are dominated by older mountain belts, Brooks Range in Alaska and Verkhoyansk Belt in Siberia (Miller et al., 2018), and thus the erosion-induced gravity correlates both qualitatively and quantitatively.

The exercise of this section illustrates a set of geodynamic points: (1) Erosion is one of the major controls of the Earth's gravity anomalies. (2) The pre-erosional topography calculated in our study has lower elevation than the modern, which is an oversimplification for orogenic areas where peaks are also subjected to erosion (opposite to our model assumption), but it illustrate that erosion keeps orogens high even after they stop being active. (3) The approach may help to resolve to what extent the topography of active orogens is controlled by tectonics and erosion. (4) The approach of this section assumes the pre-erosional configuration in the state of local isostasy, which may be an oversimplification for orogenic areas, but the pre-erosional non-isostatic signal fades as the lithosphere loses its flexural rigidity with time (Watts and Zhong, 2000; Watts et al., 2013) and the assumption may be considered as valid for ancient orogenic belts.

Several technical points also become clear: (1) EBT is applicable not only in glacially-controlled landscapes but also in orogenic areas. (2) Gravity data may be used to test EBT results and/or to control the iteration process of EBT (Appendix A). (3) The low-relief pre-erosional topography modelled with EBT loses high frequency characteristics due to numerical inversion, but it also correlates with the loss of high frequency characteristics lithospheric rigidity with time.

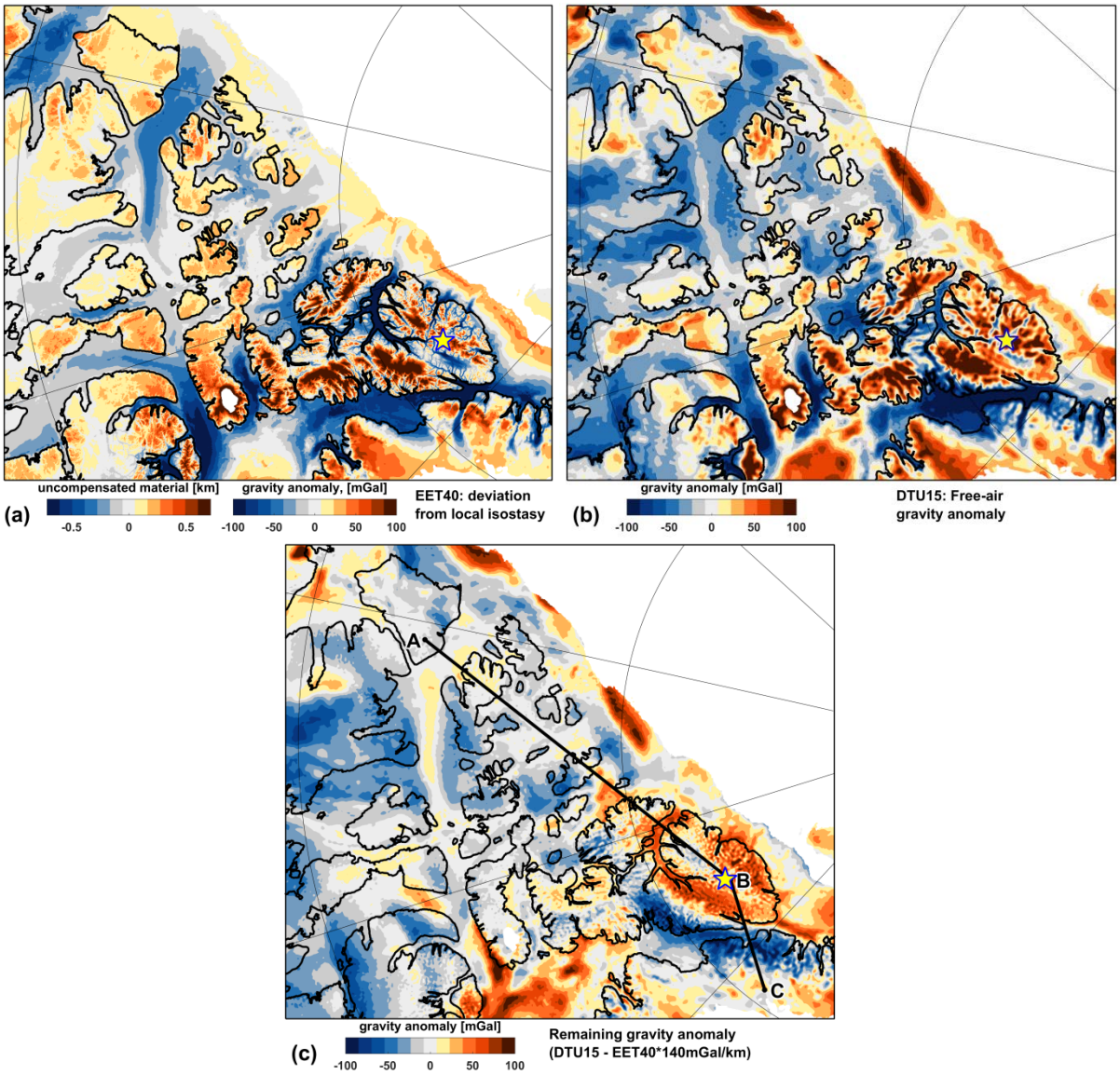

Figure 9. Relationship between modelled mass redistribution and observed gravity anomalies in the Canadian Arctic Archipelago (region 1 in Figure 5). (a) Thickness Δh of excess mass ΔM derived from model can be also expressed via corresponding gravity anomaly Δg_{EET40} (=Δh×140 mGal/km, eq. 2); (b) Free air gravity anomaly (DTU15, updated version, after Andersen, 2010; Andersen et al., 2010); (c) Difference between observed gravity signal and modelled erosion-induced gravity signal Δg_{EET40}. Line ABC shows position of profile in Figure 10.

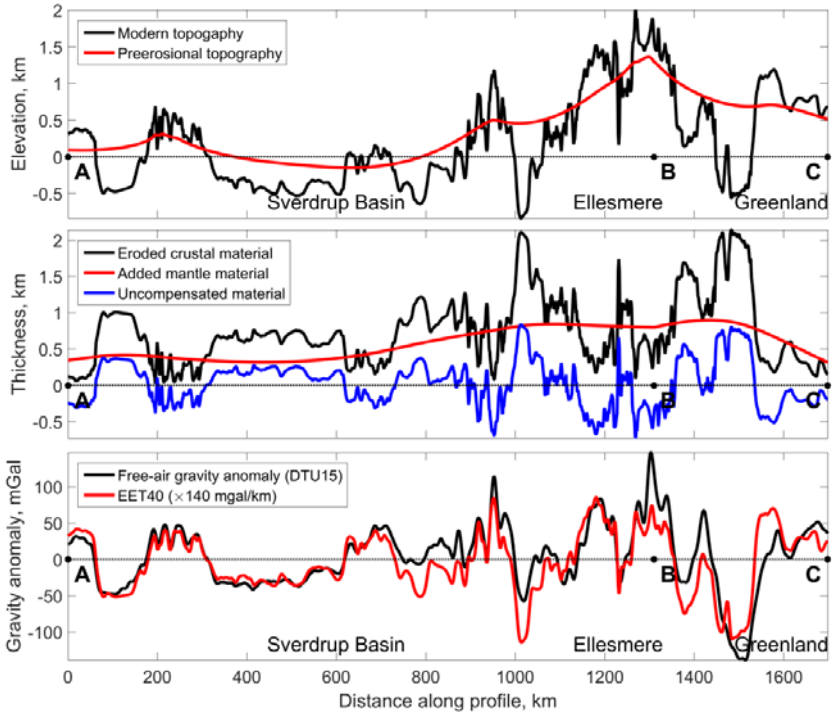

Figure 10. Profile ABC (see location in Figure 9): (a) Modern and pre-erosional (modelled) topography. (b) EBT estimates of eroded (h_e, eq. 1, black line) material, additional mantle material (h_m, red line), and excess, locally uncompensated material (Δh, blue line). (c) Comparison of observed gravity anomaly and gravity response from locally uncompensated material (smoothed Δh×140 mGal/km, eq. 2).

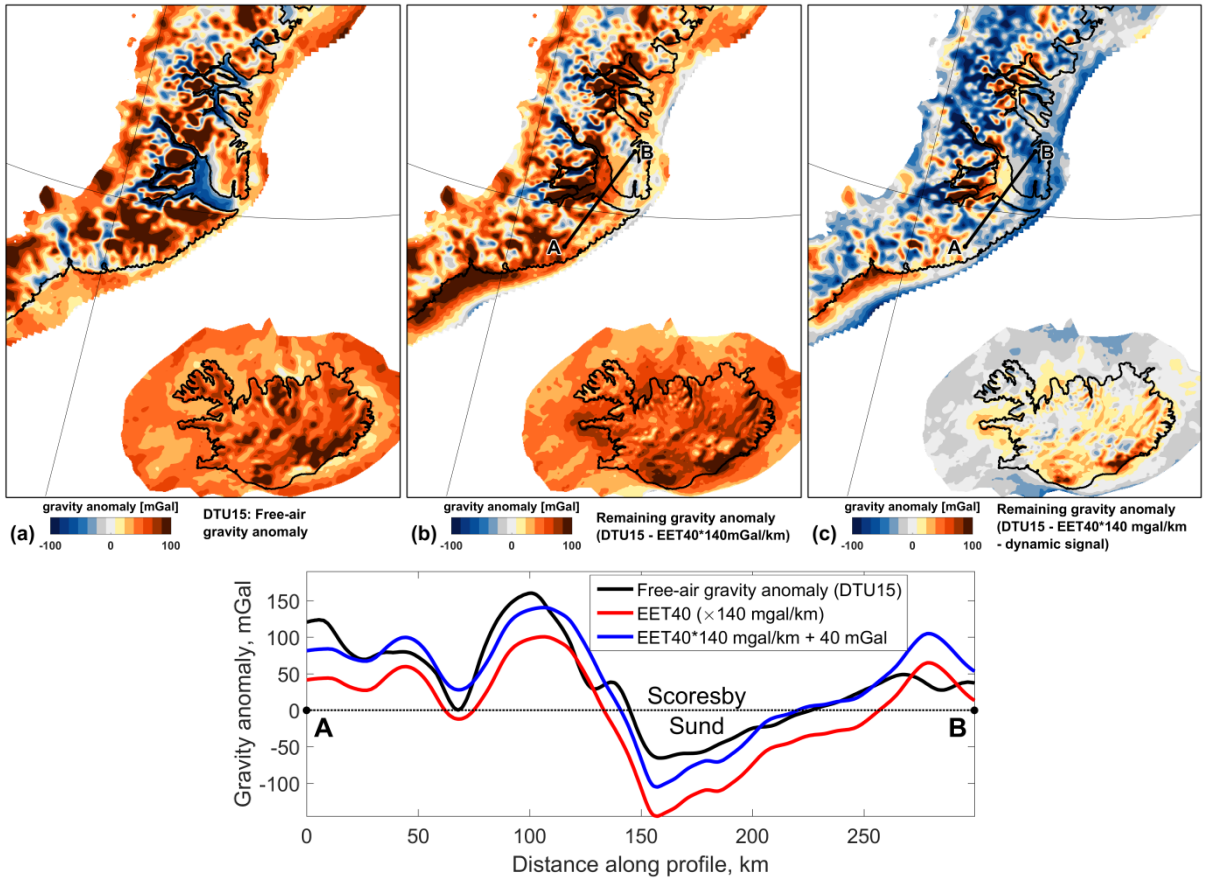

Figure 11. North Atlantic gravity analysis (region 4 in Figure 5): (a) observed free-air gravity Γ; (b) gravity explained by erosion only, Γ- Δg_{EET40}; (c) gravity explained by erosion and regional anomaly Γ- Δg_{EET40}-40 mGal; (d) profile AB (see location in c) illustrating relation of set of sources of gravity anomalies.

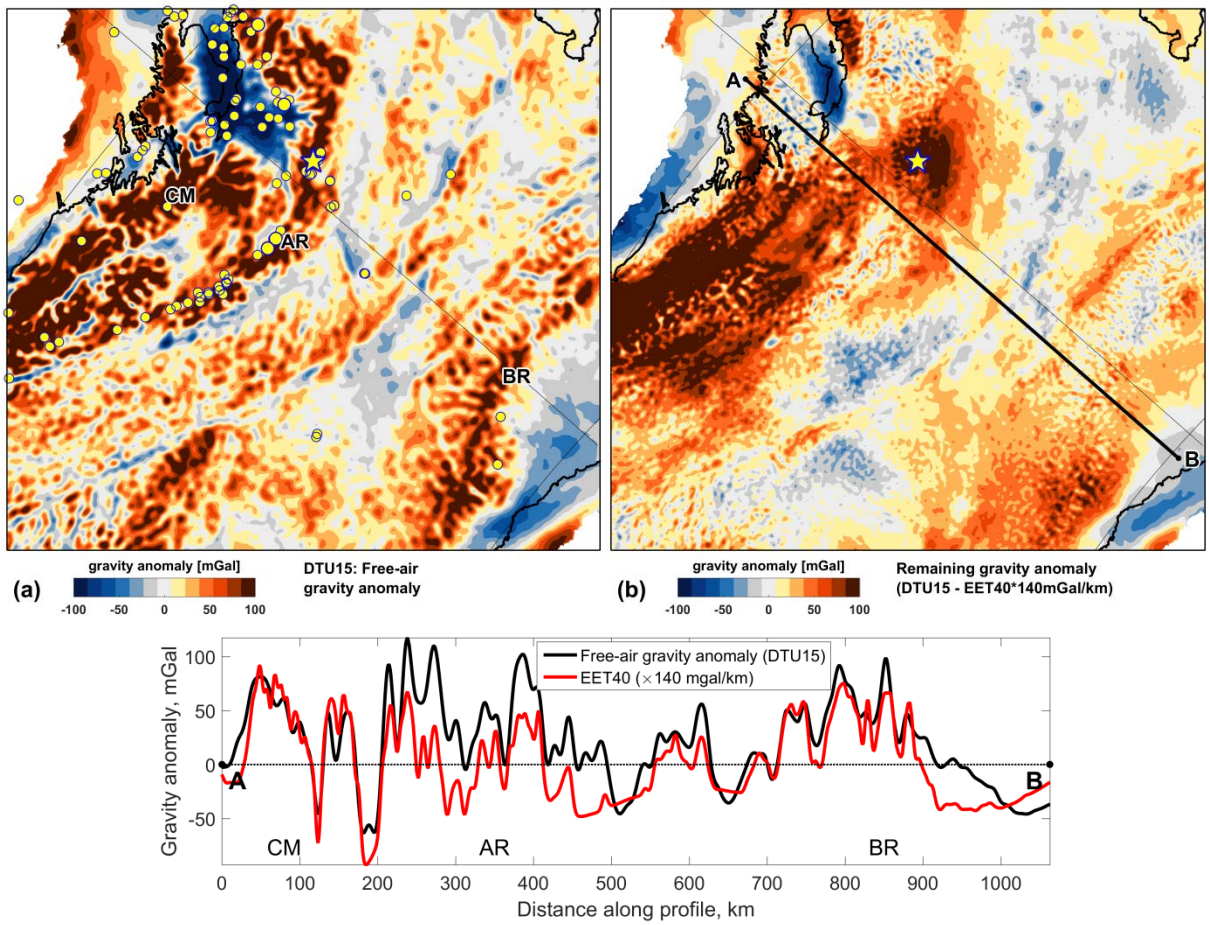

Figure 12. Gravity signal analysis for Alaska (region 2 in Figure 5) (a) free air gravity anomaly; (b) observed gravity reduced by erosion-induced signal Δg_{EET40} (eq. 2); (c) profile AB (see location in b) illustrating relation between observed and modelled erosion-induced gravity signal. Yellow circles in (a) show location of magnitude 5+ earthquakes during last 20 years (USGS Earthquake Catalog). CM=Coast Mountains, AR=Alaska Range, BR=Brooks Range.

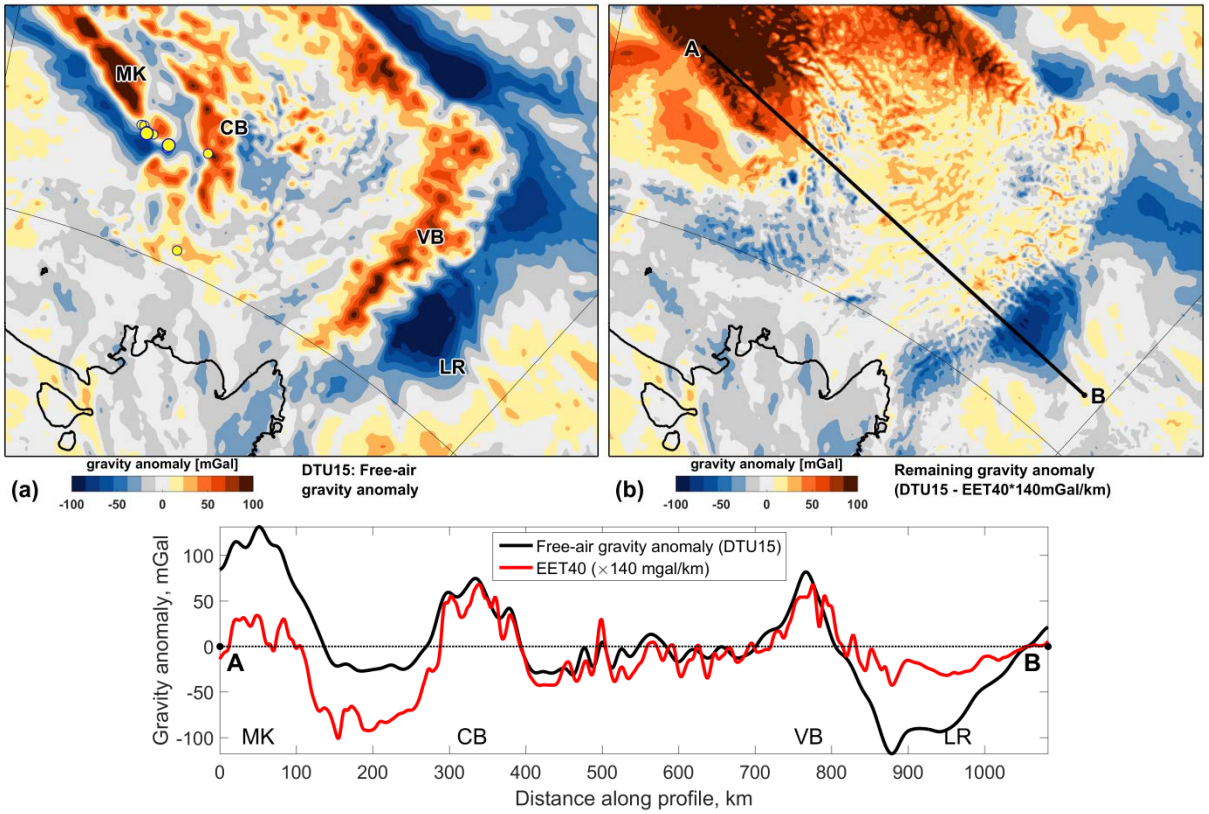

Figure 13. Gravity signal analysis for north central Siberia (region 3 in Figure 5) (a) free air gravity anomaly; (b) observed gravity reduced by erosion-induced signal Δg_{EET40} (eq. 2); (c) profile AB (see location in b) illustrating relation between observed and modelled erosion-induced gravity signal. Yellow circles in (a) show location of magnitude 5+ earthquakes during last 20 years (USGS Earthquake Catalog). LR=Lena River, VB=Verkhoyansk Belt, CB=Chersky Belt, MK=Momskiy Khrebet.

5. Conclusions

We model the influence of erosion on displacements of the circum Arctic lithosphere using the *erosion backward in time* (EBT) technique. Our results show:

1. Major vertical displacements of circum Arctic topography are caused by a non-tectonic mechanism, namely, erosion. Our study demonstrates the influence of erosion on a variety of modern landscapes of the Arctic within a single numerical formulation.
2. Localized erosion, like glacial fjord carving, combined with long-wavelength response from a strong elastic lithosphere may cause km-scale uplift of adjacent areas, as demonstrated at the Canadian Arctic Archipelago. Dominantly fluvial erosion of both old and active orogens produces even greater effects than glacial erosion. However, in such areas of active tectonics, like in southern Alaska, the EBT method should be used with caution, given that topography in part may be structural or tectonic in nature. In contrast, the erosional unloading and associated isostatic readjustment support the high elevation of older orogens.
3. Even though the erosion-induced loss of crustal material is isostatically balanced by uplift of mantle material on a regional scale, the isostasy may be misbalanced locally. This deviation results in gravity anomalies. Erosion is one of the major mechanisms controlling gravity anomalies in the Arctic. Active orogenesis (like in southern Alaska) and mantle-induced dynamic uplift (like in the north Atlantic) may affect the gravity signal, and thus analysis should be done carefully.
4. Comparison of modelling results with observed gravity anomalies supports applicability of EBT not only to glacially-control landscapes, but also to old orogenic belts subjected to intensive erosion.

5. Variations of parameters like density of eroded rocks, strength of lithosphere, and accumulation of eroded material demonstrated that if these variations are within a reasonable range, their effects are secondary.
6. Additional analysis shows that iterations between erosional and isostatic processes is the natural process imbedded in EBT and is an important component of large-scale analysis of erosional effects.

Acknowledgments

Authors acknowledge support from the Research Council of Norway through its Centers of Excellence funding scheme, project 223272. S.M. thanks AkerBP for financial support. We thank two anonymous reviewers for their helpful comments on an early version of the paper. David Egholm is thanked for providing results of his numerical model. Editorial support by Lucy Medvedeva, Muriel Gerbault, and especially by Allegra Hosford Scheirer is appreciated.

Appendix A. Iterative procedure of Erosion Backward in Time (EBT) and pre-erosional topography

A1. Comparison of EBT with forward numerical model

Advantages of EBT include the simplicity of the numerical treatment and its easy application to real landscapes. The accuracy of EBT, however, is a point of discussion. Forward numerical modelling of glacial erosion and development of fjords (e.g., Egholm et al., 2017; Kessler et al., 2008) allows testing of our approach. Here we apply EBT to reproduce a numerical experiment of Egholm et al. (2017, their fig. 2, marked as E2017 hereafter) taking the modelled fjord-dominated landscape as an initial configuration for EBT and attempting to reconstruct initial, fluvial-dominated landscape. The limited lateral extent of the model domain (100x50 km) results in insignificant (30-40 m) lateral variations of flexural isostatic adjustment, which allows us to ignore isostatic balance, concentrating chiefly on erosion and thus reducing the number of controlling characteristics to two, namely, the initial and final relief (difference between these two directly indicate amount of erosion, Figure 14a).

The iterative approach of EBT allows saving several consequent records corresponding to consecutively increased number of iterations and then search for the best-fit record. Figure 14a presents cross-section of results of EBT records (red lines) which successively filled the concave shapes of the initial fjord-like landscape (black line, the final result of E2017). Increasing number of iterations results in the increasing amount of modelled erosion, which can be compared with the average amount of ca. 0.5 km registered in E2017 (Figure 14b). This comparison determines preferential record of EBT (blue star in Figure 14b and blue line in Figure 14a). The preferential model approximates at long wavelength the initial landscape (green line in Figure 14a), and thus we conclude successful reconstruction of the pre-erosional topography with EBT.

There are, however, only few locations in the Arctic, where the volume of eroded material may be considered as known, and thus the above selection of the preferential record needs revision. Condition of saturation of iterations used in this study for control regions (Appendix A2) and in the previous applications (Medvedev and Hartz, 2015; Medvedev et al., 2013) would result in choice of the shallowest of the iteration surfaces in Figure 14a. This saturation surface accounts for glacial erosion (with good accuracy as indicated by intermediate iterations) and for preceding fluvial erosion (with somewhat lesser accuracy) and termed as the pre-erosional topography in this study. This surface may never have physically existed but it can describe the influence of the total erosion recorded in the modern topography.

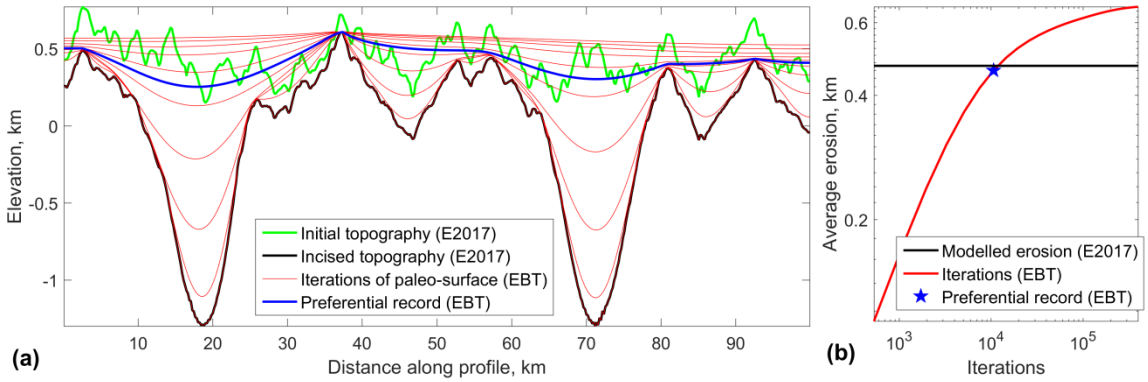

Figure 14. (a) Comparison of EBT iterative process (thin red lines sequencing from bottom up) with a forward modelling of development of fjord-dominated landscape (black line) from the initial river-type landscape (green line) performed in Egholm et al. (2017, marked as E2017). We disregard isostatic adjustment here to present erosional and EBT processes more clear. (b) Comparison of eroded masses in forward experiment (black line, E2017) with EBT iterations (red line) selects the preferential record (blue line in a and star in b).

A2. Iterative procedure of EBT and other inverse approaches

Several earlier studies quantified the influence of erosion using backward in time approaches (e.g., Champagnac et al., 2007; Schermer et al., 2017; Small and Anderson, 1998; Steer et al., 2012). Using the modern landscapes, these studies estimate the amount of eroded material but do not account for additional development of landscapes caused by isostatic readjustment. In contrast, EBT iterates between filling the concave shapes and isostatic readjustment of the system, thus resulting in the pre-erosional topography.

The open question in our method is the termination criterion for the iterative process. Previous studies were operating with intermediate length scales of generally convex shapes (e.g., Greenland and Scandinavian mountain range bounded by seas) which fast resulted in the saturation of iterations in EBT and a low significance of a particular termination criterion (area 3 in Figure 15). The Arctic region analyzed in this study is of much larger size and has a large variety of morphology. The special concern here is the large-scale depression like the Sverdrup Basin in the Canadian Arctic Archipelago (Area 2 in Figure 15). Whereas areas 1 and 3, characterized by strong relief, is smoothed within the first part of iterations (Figure 15a to b) and shows only minor changes in subsequent ones (Figure 15c), area 2 continues to change by deepening the depression during the first part of the iterations (Figure 15b) and then fills this depression finally raising it above sea level (Figure 15c). The general styles of evolution produced by EBT for these areas are illustrated in Figure 16a, where the amount of added material saturates for areas 1 and 3 and continuously grows for area 2. Thus, the stopping criteria used in our previous works must be adjusted when applied for the broader Arctic realm.

Figure 16b presents the evolution of variations of topography for areas 1 and 2, measuring the difference between maximum and minimum elevation. The graphs demonstrate that the topography variations saturate for both areas after a certain number of iterations, after which the process acts on scale larger than 500-600 km, characteristic size of areas 1 and 2. That gives us an indicator for stopping the iterative process and selects the preferential record. Figure 17 shows that the style of EBT changes over preferential record: the initial set of records (green lines; prior to the preferential record) results in smooth topography, whereas post-preferential records simply fills in the large-scale depression of the Sverdrup Basin (red lines). The choice of the length-scale of testing boxes (400-600 km) is supported by the global gravity study (Watts and Moore, 2017), which shows that the larger scale is likely to be balanced isostatically on average.

Figure 16c considers a counter-intuitive effect of erosion, that is, topography rise of the areas adjacent to localized erosion. Generally, the more material that is added into the system during EBT, the stronger this effect is. However, the effect is reduced for the records beyond the preferential record, even for area 2 (although masses added are significant, Figure 16a), indicating suitable choice of the preferential record. Secondly, even if we reduce mass that is input to EBT by stopping iterations earlier,

the effect is still visible. Thus, reducing mass input by 30% will result in effect decrease only by ca. 20%.

Previous studies also used two methods that differ from EBT. Whereas the interpolation of the low relief surfaces method (Small and Anderson, 1998; Steer et al., 2012) assumes peneplained summit topography and is thus unlikely applicable to the large-scale dimensions in our study, we can compare our restoration with the geophysical relief method (Champagnac et al., 2007; Steer et al., 2012). The latter method is based on an assumption that for any window of a certain radius *R* within a domain there is at least one elevated point which was not affected by erosion; enveloping these points constrains the pre-erosional topography. This assumption makes the method strongly dependent on *R* and has limited applicability if the length scale of landforms are comparable or larger than *R*. Application to western Alps by Champagnac et al. (2007) sets *R*=3 km, whereas Steer et al. (2012) shows that range of *R*=1-7 km may lead to completely different conclusions. The best fit to example of Appendix A1, with landform length scale of 10-20 km, is achieved using *R*=10 km. Comparison of results for the areas 1 and 3 in Figure 16a shows that EBT is capable handling landscapes of different length scales as smaller scale system (like area 3) saturates fast and then is not affected significantly by continued iterations.

Figure 18 compares the EBT and geophysical relief methods and illustrates the importance of simultaneous iterations for filling the concave shapes and isostatic readjustment. The preferred model (blue line) aims to smooth topography after isostatic adjustment, and thus it does not look appropriate on the graph before adjustment (cf. Figure 18 a and b). The plot also shows that the values of *R* used in the previous studies for much smaller scales of landforms do not perform well for the case of the entire Arctic, as even *R*=50 km cannot smooth out the Nares Strait, which separates the Ellesmere Island from Greenland. Our preferred model also accounts for 0.5-1 km more erosion in the area of Nares Strait (Figure 18a) although the difference is not as visible after isostatic adjustment (Figure 18b).

Analysis similar to Figure 16 applied to orogens (areas 2 and 3 in Figure 5) does not show saturation in any of the considered measures, indicating interaction of orogenic and erosional landscape-forming effects. Thus, these regions do not control termination of EBT iterations in our whole-Arctic model. The analysis of the gravity anomalies (Figure 9-Figure 13), however, supports the chosen approach. In general, more accurate analysis of erosional process requires regional investigations which can bring understanding of the stopping criteria for EBT iterations; orogenic areas set additional challenges.

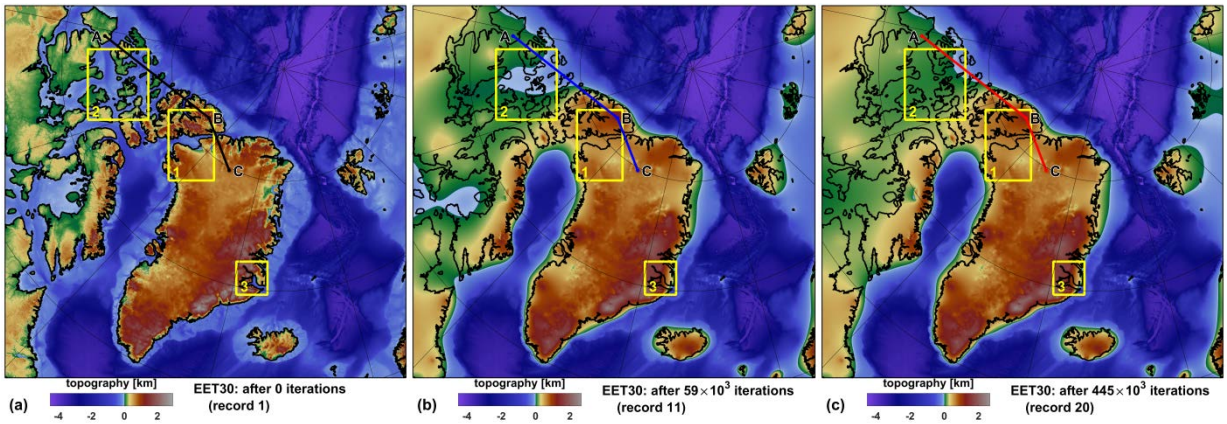

Figure 15. Initial (modern) topography (a) and two records of iteration process of EBT (preferential 11th record, b, and one of the final records, 20th, c). Three areas outlined by yellow squares (area 1 covers part of Ellesmere Island and NW Greenland, area 2 covers the central part of Canadian Arctic Archipelago, the Sverdrup Basin, and area 3 includes Scoresby Sund) are analyzed in Figure 16. The color variations of profile ABC (black on a, blue on b, and red on c) correspond to the presentation of this profile in Figure 17.

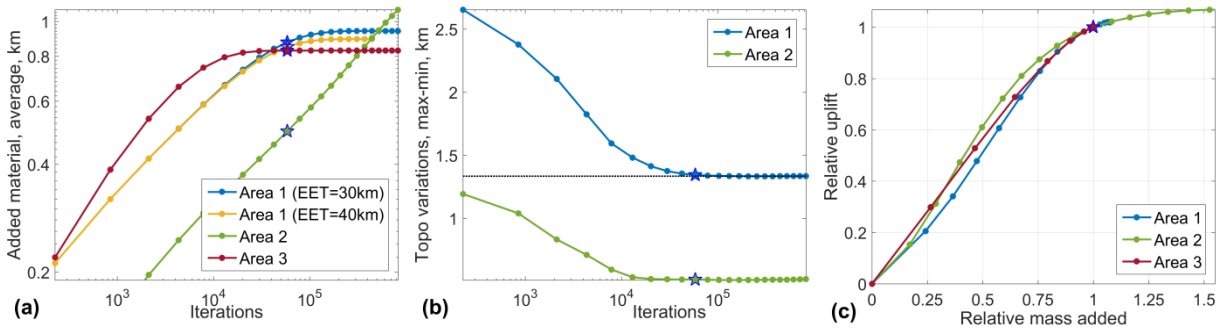

Figure 16. Integrated analysis of areas outlined in Figure 15: (a) amount of added material during EBT averaged over the corresponding area; and, (b) evolution of topography variations (difference in elevation between highest and lowermost points within each area) during EBT iterations. (c) Evolution of uplifted parts (more than 0.2 km elevation rise caused by erosion) vs. added mass (both variables are scaled by the corresponding values at the preferential record). The preferential record is marked by a star.

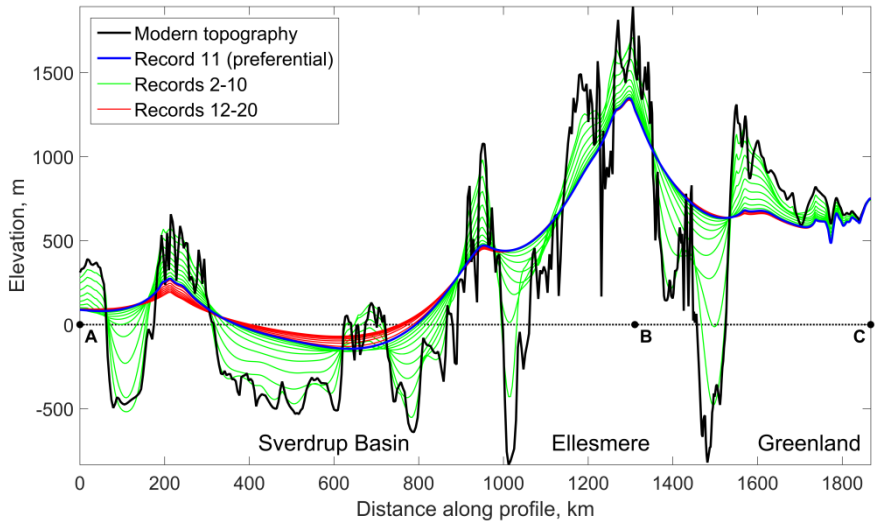

Figure 17. Evolution of topography during EBT iterations starting with modern topography (black) through a set of intermediate steps (green lines) to preferential record (blue) and further to iterations that we consider as overfill (red lines). Note that the red lines saturate around the blue line of preferential record in the Ellesmere-Greenland part of profile, whereas the Sverdrup Basin, with a general large-scale depression shape, continues to fill during later iterations. See location of profile ABC in Figure 15.

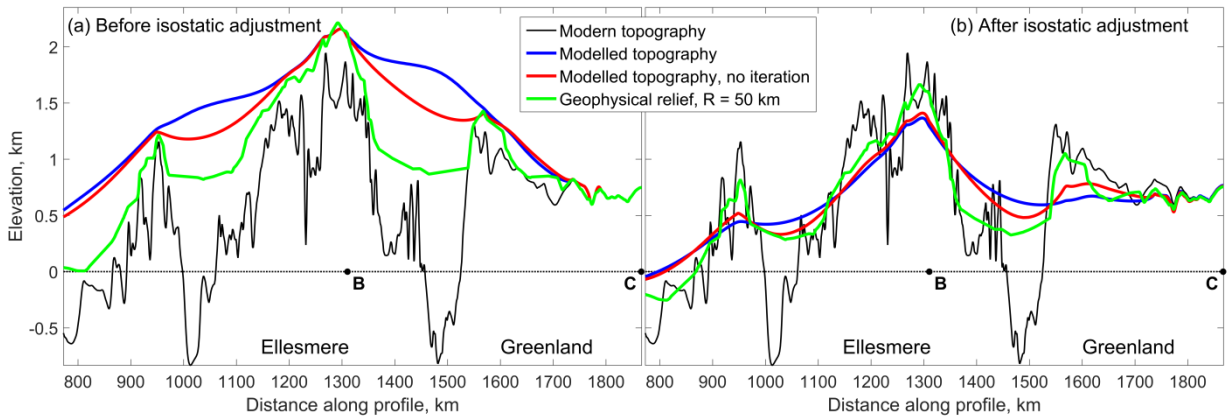

Figure 18. Comparison of different methods to reconstruct the pre-erosional topography before isostatic readjustment (a) and after (b). All the fill-in methods envelop the modern topography before readjustment (a), but move down after isostatic readjustment caused by additional loading. Comparison of blue (preferred EBT model) and red lines (model that fills concave shapes without simultaneous isostatic iterations) shows that the model without iterations is smoother before isostatic adjustment, but creates additional concave shapes on the final adjusted topography (see fjords bordering Ellesmere Island). The geophysical relief method, even applied with a large radius of 50 km, does not fill the fjords. The models presented here use EET=20 km. The profile position corresponds to 770 to 1800 km of ABC profile in Figure 17.

Appendix B. Influence of offshore sedimentation

In this section we analyze how much ignoring the off-shore sediment accumulation affects the on-land's vertical motions predicted in the previous sections. We consider a single sedimentary succession in the Lincoln Sea, which may be associated with material eroded in the Nares Strait, a strong erosional feature between Ellesmere Island and Greenland (Dawes, 2009). The sedimentary map of the Arctic (Petrov et al., 2016) shows sediments in this region that are up to 11.7 km thick (Figure 19).

Vogt et al. (1998) pointed out that young (mainly Quaternary) offshore sediments, dominantly associated with deltas of active ice streams of recent and former glaciations, show positive free-air gravity anomalies. The gravity data indeed shows a strong anomaly in the Lincoln Sea (Figure 19). Seismic studies and gravity modelling (Jackson and Dahl-Jensen, 2010; Sørensen et al., 2011) demonstrate that the sediments are of at least two different depositional episodes and that the younger sediments, probably associated with glacial erosion, were accumulated on the northern edge of that basin and do not exceed 5 km in thickness.

Figure 20 presents the results of two numerical experiments in which the sediment succession of the Lincoln Sea was separated into two parts. The bottom 5 km was treated as "old sediments" and was not taken into account, whereas the upper part (up to 6.7 km) was assumed as an external load. Considering the larger portion of sediments as related to gvlacial erosion (>6 compared to 5 km in Jackson and Dahl-Jensen, 2010; Sørensen et al., 2011), and shifting the depocenter of this succession closer to the land (if we assume that maximum gravity anomaly corresponds to the main part of the young sediments, Figure 19), these experiments provide an upper limit of impact of sediment accumulation related to glacial erosion. The results presented for the two different EET show that this impact is limited to coastal areas and its amplitude is smaller than that of erosion.

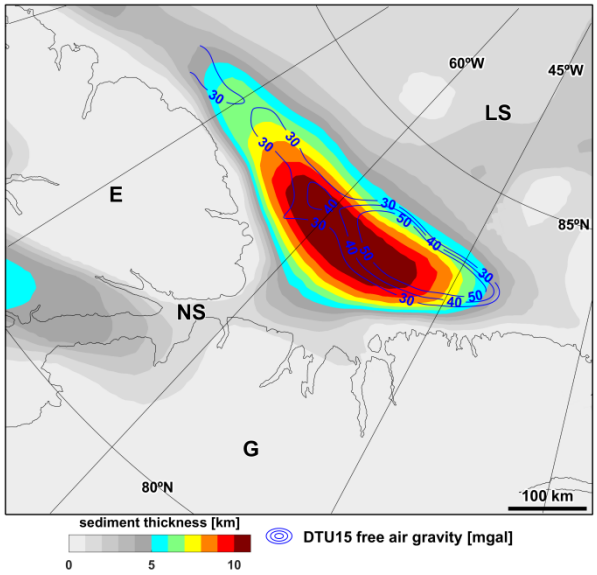

Figure 19. Thickness of sediments (Petrov et al., 2016) with free-air gravity anomaly isolines (DTU15, updated after Andersen, 2010; Andersen et al., 2010). The model assumes that the bottom 5 km of sediments (marked by gray shades) are older sediments, whereas up to ~6.5 km (colors) are sediments accumulated due to glacial erosion. See location of the region in Figure 3. E=Ellesmere Island, G=Greenland, LS=Lincoln Sea, NS=Nares Strait.

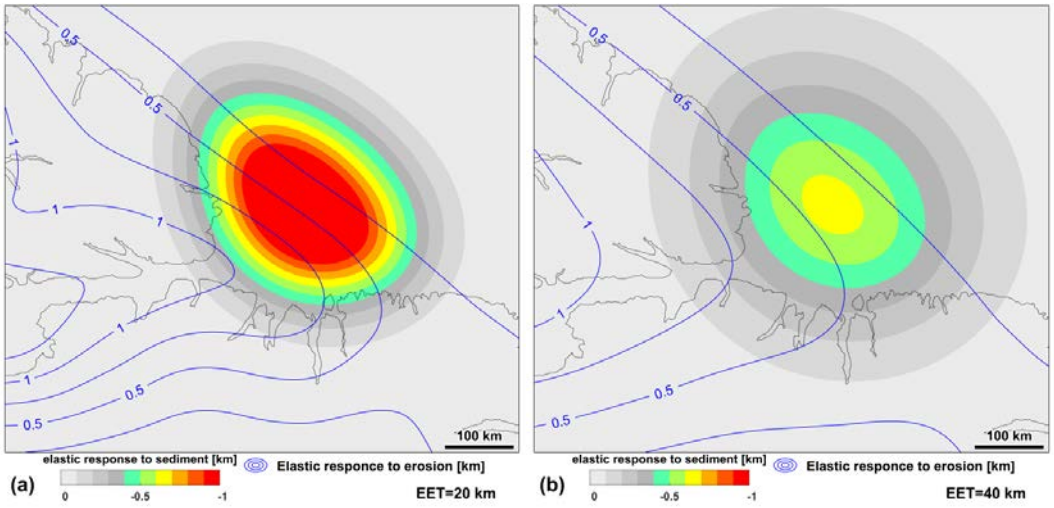

Figure 20. Results of numerical calculations of elastic isostatic response to loading of a sedimentary delta of the Lincoln Sea for EET 20 km (a) and 40 km (b). The colors are chosen to emphasize the influence of sediment accumulation on on-shore vertical movements, which is generally <400 m and extends by less than 100 km. Blue isolines illustrate the results of the EBT (see also Figure 4b). Note that considering forward in time evolution, the elastic response to sedimentation is downward movements, whereas erosion results in uplift.

Appendix C. Influence of rheological variations

Figure 21 compares the results of the models with EET of 20 and 40 km. Similar to conclusions made in Medvedev and Hartz (2015), although the amplitudes of erosion (Figure 21a) and elastic response (Figure 21b) are somewhat different, qualitatively, these two processes are the same in both models. Comparison of pre-erosional topographies (Figure 21c) shows that landscape evolutions are similar, even in a quantitative way. In particular, little difference is observed in the Canadian Arctic Archipelago. We attribute the independence of topography from rheology of the lithosphere in this area to the population of large fjords, which are denser than the characteristic wavelength of elastic plates in a 20-40 km thickness range.

We also study the influence of lateral variations of EET. Our study does not intend to utilize patchy and yet imprecise models for EET distributions in the Arctic, but it does illustrate the potential influence of lateral variations of EET by the most typical mechanism of lithosphere weakening: hot mid-oceanic ridge (MOR). Two models are compared here, EET40 and EET40/5. Both have the same initial set-up and boundary conditions (Figure 3), but have different rheological properties. Whereas the EET40 model has uniform EET=40 km; EET of the EET40/5 model depends on the proximity to mid-oceanic ridge, ranging from 5 km for the young oceanic lithosphere to 40 km for the areas 5 arc degrees away from the ridge (Figure 22). This test was designed to estimate the potential influence of weakened lithosphere and thus accuracy of approximation is not crucial.

Model results indicate that effects of rheological changes are only important locally. Comparison of the two model results (Figure 23) shows how the interaction between erosion and flexural isostatic adjustment depend on the distance to the MOR. Placed-in material (Figure 23a) is more massive in the model with variable EET, suggesting that erosion is more favorable/stronger in the areas weakened by heat from the MOR. Thus, the lithosphere under East Greenland and Svalbard are uplifted more in the model with variable EET (Figure 23b). Pre-erosional topography predicted by the model with variable EET is lower in East Greenland, Iceland, and Svalbard (Figure 23c).

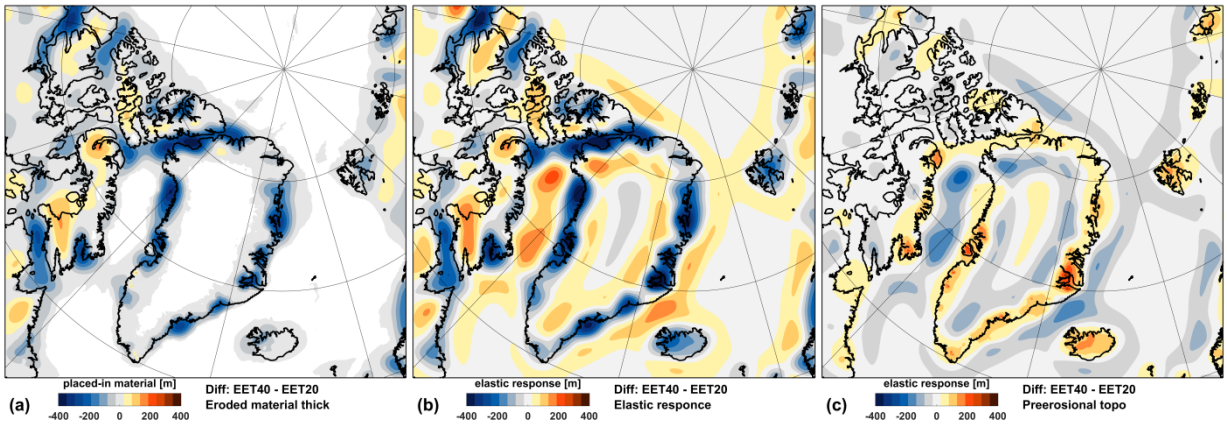

Figure 21. Difference in results between models with different EET: EET40 (EET=40 km, Figure 4) and EET20 (EET=20 km).

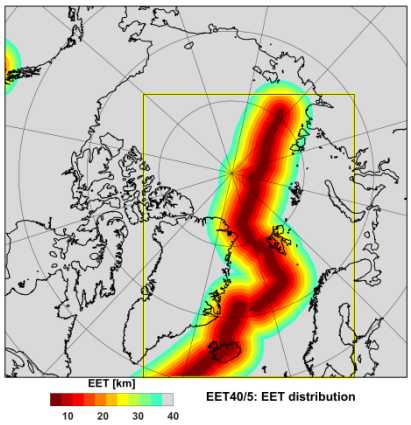

Figure 22. EET map for the model EET40/5. EET increases linearly from a minimum of 5 km at the roaching mid-oceanic ridge (Figure 1) to 40 km at a distance of 5º away.. Yellow box outlines area where results are visibly different from the uniform EET model (Figure 23).

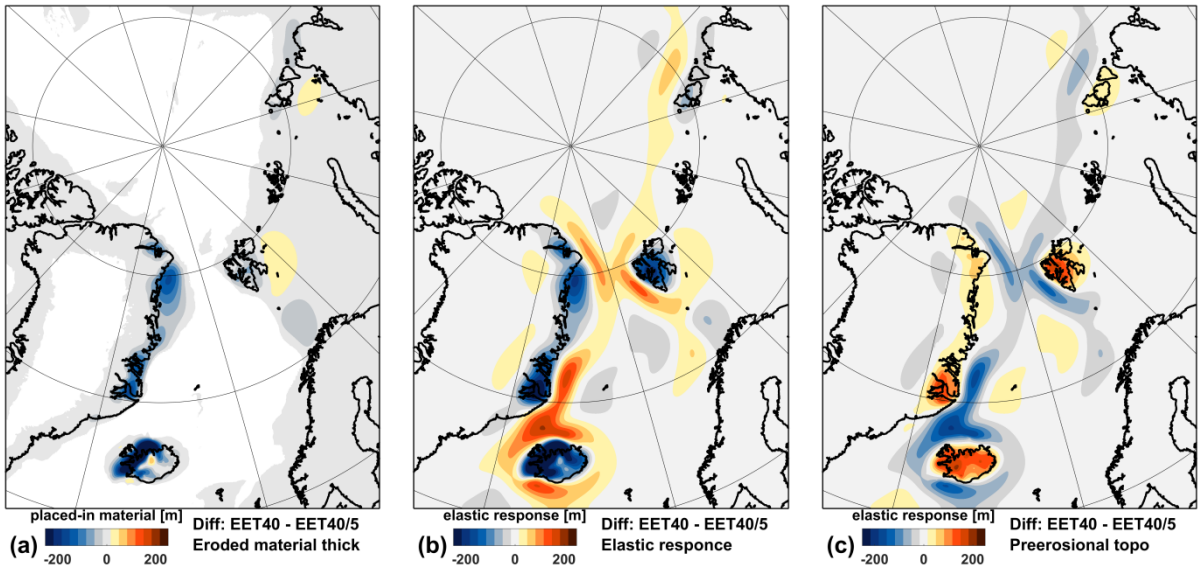

Figure 23. Comparison of placed-in material (a), elastic response (b) and the final topography (c) by subtracting results of model EET40/5 (Figure 22, variable EET) from EET40 (Figure 4, uniform EET).

References

Amante, C., Eakins, B.W., 2009. ETOPO1 1 arc-minute global relief model: procedures, data sources and analysis. US Department of Commerce, National Oceanic and Atmospheric Administration, National Environmental Satellite, Data, and Information Service, National Geophysical Data Center, Marine Geology and Geophysics Division Colorado.

Andersen, J.L., Egholm, D.L., Knudsen, M.F., Linge, H., Jansen, J.D., 2016. Erosion of mountain plateaus along Sognefjord, Norway, constrained by cosmogenic nuclides, EGU General Assembly Conference Abstracts p. 9915.

Andersen, O., 2010. The DTU10 gravity field and mean sea surface, Second international symposium of the gravity field of the Earth (IGFS2), Fairbanks, Alaska, pp. 20-22.

Andersen, O.B., Knudsen, P., Berry, P.A., 2010. The DNSC08GRA global marine gravity field from double retracked satellite altimetry. Journal of Geodesy 84, 191-199.

Auriac, A., Whitehouse, P., Bentley, M., Patton, H., Lloyd, J., Hubbard, A., 2016. Glacial isostatic adjustment associated with the Barents Sea ice sheet: A modelling inter-comparison. Quaternary Sci Rev 147, 122-135.

Baig, I., Faleide, J.I., Jahren, J., Mondol, N.H., 2016. Cenozoic exhumation on the southwestern Barents Shelf: Estimates and uncertainties constrained from compaction and thermal maturity analyses. Mar Petrol Geol 73, 105-130.

Becker, J.J., Sandwell, D.T., Smith, W.H.F., Braud, J., Binder, B., Depner, J., Fabre, D., Factor, J., Ingalls, S., Kim, S.H., Ladner, R., Marks, K., Nelson, S., Pharaoh, A., Trimmer, R., Von Rosenberg, J., Wallace, G., Weatherall, P., 2009. Global bathymetry and elevation data at 30 arc seconds resolution: SRTM30_PLUS. Mar Geod 32, 355-371.

Brush, D.O., Almroth, B.O., 1975. Buckling of bars, plates, and shells. McGraw-Hill, New York.

Buchan, K.L., Ernst, R., 2006. Giant dyke swarms and the reconstruction of the Canadian Arctic islands, Greenland, Svalbard and Franz Josef Land. Dyke swarms: time markers of crustal evolution, 27-48.

Champagnac, J., Molnar, P., Anderson, R., Sue, C., Delacou, B., 2007. Quaternary erosion-induced isostatic rebound in the western Alps. Geology 35, 195-198.

Cocks, L.R.M., Torsvik, T.H., 2011. The Palaeozoic geography of Laurentia and western Laurussia: a stable craton with mobile margins. Earth-Science Reviews 106, 1-51.

Coney, P.J., Jones, D.L., Monger, J.W., 1980. Cordilleran suspect terranes. Nature 288, 329-333.

Conrad, C.P., Lithgow-Bertelloni, C., Louden, K.E., 2004. Iceland, the Farallon slab, and dynamic topography of the North Atlantic. Geology 32, 177-180.

Dawes, P.R., 2009. Precambrian–Palaeozoic geology of Smith Sound, Canada and Greenland: key constraint to palaeogeographic reconstructions of northern Laurentia and the North Atlantic region. Terra Nova 21, 1-13.

Eberhart-Phillips, D., Haeussler, P.J., Freymueller, J.T., Frankel, A.D., Rubin, C.M., Craw, P., Ratchkovski, N.A., Anderson, G., Carver, G.A., Crone, A.J., 2003. The 2002 Denali fault earthquake, Alaska: a large magnitude, slip-partitioned event. Science 300, 1113-1118.

Egholm, D.L., Jansen, J.D., Brædstrup, C.F., Pedersen, V.K., Andersen, J.L., Ugelvig, S.V., Larsen, N.K., Knudsen, M.F., 2017. Formation of plateau landscapes on glaciated continental margins. Nat Geosci 10, 592.

Fitzgerald, P.G., Stump, E., Redfield, T.F., 1993. Late Cenozoic uplift of Denali and its relation to relative plate motion and fault morphology. Science 259, 497-497.

Flament, N., Gurnis, M., Müller, R.D., 2013. A review of observations and models of dynamic topography. Lithosphere 5, 189-210.

Fowler, C., 1990. The Solid Earth: An Introduction to Global Geophysics. Cambridge University Press.

Fuis, G.S., Moore, T.E., Plafker, G., Brocher, T.M., Fisher, M.A., Mooney, W.D., Nokleberg, W.J., Page, R.A., Beaudoin, B.C., Christensen, N.I., 2008. Trans-Alaska Crustal Transect and continental evolution involving subduction underplating and synchronous foreland thrusting. Geology 36, 267-270.

Gac, S., Klitzke, P., Minakov, A., Faleide, J.I., Scheck-Wenderoth, M., 2016. Lithospheric strength and elastic thickness of the Barents Sea and Kara Sea region. Tectonophysics 691, 120-132.

Gaina, C., Medvedev, S., Torsvik, T.H., Koulakov, I., Werner, S.C., 2014. 4D Arctic: A glimpse into the structure and evolution of the Arctic in the light of new geophysical maps, plate tectonics and tomographic models. Surveys in Geophysics 35, 1095-1122.

Gaina, C., Nasuti, A., Kimbell, G.S., Blischke, A., 2017. Break-up and seafloor spreading domains in the NE Atlantic. Geol. Soc. London Spec. Pub. 447, SP447. 412.

Grantz, A., Hart, P.E., Childers, V.A., 2011. Geology and tectonic development of the Amerasia and Canada Basins, Arctic Ocean. Geol. Soc. London, Memoirs 35, 771-799.

Harrison, J.C., St-Onge, M.R., Petrov, O.V., Streinikov, S.I., Lopatin, B.G., Wilson, F.H., Tella, S., Paul, D., Lynds, T., Shokalsky, S.P., Hults, C.K., Bergman, S., Jepsen, H.F., Solli, A., 2011. Geological Map of the Arctic: Carte Géologique de L'Arctique. Geological Survey of Canada

Henriksen, E., Bjørnseth, H., Hals, T., Heide, T., Kiryukhina, T., Kløvjan, O., Larssen, G., Ryseth, A., Rønning, K., Sollid, K., 2011. Uplift and erosion of the greater Barents Sea: impact on prospectivity and petroleum systems. Geol. Soc. London, Memoirs 35, 271-281.

Jackson, H.R., Dahl-Jensen, T., 2010. Sedimentary and crustal structure from the Ellesmere Island and Greenland continental shelves onto the Lomonosov Ridge, Arctic Ocean. Geophys. J. Int. 182, 11-35.

Japsen, P., Chalmers, J.A., 2000. Neogene uplift and tectonics around the North Atlantic: overview. Global and Planetary Change 24, 165-173.

Kessler, M.A., Anderson, R.S., Briner, J.P., 2008. Fjord insertion into continental margins driven by topographic steering of ice. Nat Geosci 1, 365.

Klitzke, P., Faleide, J., Scheck-Wenderoth, M., Sippel, J., 2015. A lithosphere-scale structural model of the Barents Sea and Kara Sea region. Solid Earth 6, 153-172.

Klitzke, P., Sippel, J., Faleide, J.I., Scheck-Wenderoth, M., 2016. A 3D gravity and thermal model for the Barents Sea and Kara Sea. Tectonophysics 684, 131-147.

Koppes, M.N., Montgomery, D.R., 2009. The relative efficacy of fluvial and glacial erosion over modern to orogenic timescales. Nat Geosci 2, 644-647.

Kwon, Y.W., Bang, H., 2000. The finite element method using MATLAB, 2nd ed. CRC Press, Boca Raton, FL.

Lawver, L.A., Muller, R.D., 1994. Iceland Hotspot Track. Geology 22, 311-314.

Medvedev, S., 2016. Understanding lithospheric stresses: systematic analysis of controlling mechanisms with applications to the African Plate. Geophys. J. Int. 207, 393-413.

Medvedev, S., Hartz, E.H., 2015. Evolution of topography of post-Devonian Scandinavia: Effects and rates of erosion. Geomorphology 231, 229-245.

Medvedev, S., Hartz, E.H., Podladchikov, Y.Y., 2008. Vertical motions of the fjord regions of central East Greenland: Impact of glacial erosion, deposition, and isostasy. Geology 36, 539-542.

Medvedev, S., Souche, A., Hartz, E.H., 2013. Influence of ice sheet and glacial erosion on passive margins of Greenland. Geomorphology 193, 36-46.

Miller, E.L., Meisling, K.E., Akinin, V.V., Brumley, K., Coakley, B.J., Gottlieb, E.S., Hoiland, C.W., O'Brien, T.M., Soboleva, A., Toro, J., 2018. Circum-Arctic Lithosphere Evolution (CALE) Transect C: displacement of the Arctic Alaska–Chukotka microplate towards the Pacific during opening of the Amerasia Basin of the Arctic. Geol. Soc. London Spec. Pub. 460, 57-120.

Minakov, A., 2018. Late Cenozoic lithosphere dynamics in Svalbard: interplay of glaciation, seafloor spreading and mantle convection? J. of Geodynamics (this issue).

Minakov, A., Faleide, J.I., Glebovsky, V.Y., Mjelde, R., 2012. Structure and evolution of the northern Barents-Kara Sea continental margin from integrated analysis of potential fields, bathymetry and sparse seismic data. Geophys. J. Int. 188, 79-102.

Molnar, P., England, P.C., Jones, C.H., 2015. Mantle dynamics, isostasy, and the support of high terrain. J. Geophys. Res. 120, 1932-1957.

Muller, R.D., Sdrolias, M., Gaina, C., Roest, W.R., 2008. Age, spreading rates, and spreading asymmetry of the world's ocean crust. Geochem Geophy Geosy 9, 100-120.

Nielsen, S.B., Gallagher, K., Leighton, C., Balling, N., Svenningsen, L., Jacobsen, B.H., Thomsen, E., Nielsen, O.B., Heilmann-Clausen, C., Egholm, D.L., Summerfield, M.A., Clausen, O.R., Piotrowski, J.A., Thorsen, M.R., Huuse, M., Abrahamsen, N., King, C., Lykke-Andersen, H., 2009. The evolution of western Scandinavian topography: A review of Neogene uplift versus the ICE (isostasy-climate-erosion) hypothesis. J Geodyn 47, 72-95.

Parfenov, L., Koz'min, B., Grinenko, O., Imaev, V., Imaeva, L., 1988. Geodynamics of the Chersky seismic belt. J Geodyn 9, 15-37.

Patton, H., Andreassen, K., Bjarnadóttir, L.R., Dowdeswell, J.A., Winsborrow, M., Noormets, R., Polyak, L., Auriac, A., Hubbard, A., 2015. Geophysical constraints on the dynamics and retreat of the Barents Sea ice sheet as a paleobenchmark for models of marine ice sheet deglaciation. Rev Geophys 53, 1051-1098.

Pease, V., Drachev, S., Stephenson, R., Zhang, X., 2014. Arctic lithosphere — A review. Tectonophysics 628, 1-25.

Peltier, W.R., 2004. Global glacial isostasy and the surface of the ice-age earth: The ice-5G (VM2) model and grace. Annu Rev Earth Pl Sc 32, 111-149.

Petrov, O., Morozov, A., Shokalsky, S., Kashubin, S., Artemieva, I.M., Sobolev, N., Petrov, E., Ernst, R.E., Sergeev, S., Smelror, M., 2016. Crustal structure and tectonic model of the Arctic region. Earth-Science Reviews 154, 29-71.

Piepjohn, K., von Gosen, W., Tessensohn, F., 2016. The Eurekan deformation in the Arctic: an outline. J. Geol. Soc. 173, 1007-1024.

Prokopiev, A., 2000. Verkhoyansk-Cherskiy collisional orogen. Geology of the Pacific Ocean 15, 891-904.

Schermer, E.R., Redfield, T.F., Indrevær, K., Bergh, S.G., 2017. Geomorphology and topography of relict surfaces: the influence of inherited crustal structure in the northern Scandinavian Mountains. J. Geol. Soc. 174, 93-109.

Schiffer, C., Nielsen, S., 2016. Implications for anomalous mantle pressure and dynamic topography from lithospheric stress patterns in the North Atlantic Realm. J Geodyn 98, 53-69.

Small, E.E., Anderson, R.S., 1998. Pleistocene relief production in Laramide mountain ranges, western United States. Geology 26, 123-126.

Sobolev, P., 2012. Cenozoic uplift and erosion of the Eastern Barents Sea–constraints from offshore well data and the implication for petroleum system modelling [Känozoische Hebung und Erosion der östlichen Barentssee–Abschätzungen aus Offshore-Bohrungsdaten und Auswirkung auf die Erdölsystem-Modellierung)]. Zeitschrift der Deutschen Gesellschaft für Geowissenschaften 163, 309-324.

Steer, P., Huismans, R.S., Valla, P.G., Gac, S., Herman, F., 2012. Bimodal Plio-Quaternary glacial erosion of fjords and low-relief surfaces in Scandinavia. Nat Geosci 5, 635-639.

Struijk, M., Tesauro, M., Lebedeva-Ivanova, N., Beekman, F., Gaina, C., Cloetingh, S., 2016. Lithospheric thermal and strength model of the Arctic region, EGU General Assembly Conference Abstracts, p. 15582.

Sørensen, K., Gautier, D., Pitman, J., Jackson, H.R., Dahl-Jensen, T., 2011. Chapter 44 Geology and petroleum potential of the Lincoln Sea Basin, offshore North Greenland. Geol. Soc. London, Memoirs 35, 673-684.

Torsvik, T.H., Carlos, D., Mosar, J., Cocks, L.R.M., Malme, T.N., 2002. Global reconstructions and North Atlantic paleogeography 440 Ma to recent. BATLAS—Mid Norway plate reconstruction atlas with global and Atlantic perspectives, 18-39.

Torsvik, T.H., Cocks, L.R.M., 2016. Earth history and palaeogeography. Cambridge University Press.

Torsvik, T.H., Van der Voo, R., Preeden, U., Mac Niocaill, C., Steinberger, B., Doubrovine, P.V., van Hinsbergen, D.J., Domeier, M., Gaina, C., Tohver, E., 2012. Phanerozoic polar wander, palaeogeography and dynamics. Earth-Science Reviews 114, 325-368.

Turcotte, D.L., Schubert, G., 2002. Geodynamics, 2nd ed. Cambridge University Press, Cambridge, New York.

Veevers, J., 2004. Gondwanaland from 650–500 Ma assembly through 320 Ma merger in Pangea to 185–100 Ma breakup: supercontinental tectonics via stratigraphy and radiometric dating. Earth-Science Reviews 68, 1-132.

Vogt, P.R., Jung, W.-Y., Brozena, J., 1998. Arctic margin gravity highs: Deeper meaning for sediment depocenters? Marine Geophysical Researches 20, 459-477.

Watts, A., Moore, J., 2017. Flexural isostasy: Constraints from gravity and topography power spectra. J. Geophys. Res. 122, 8417-8430.

Watts, A., Zhong, S., 2000. Observations of flexure and the rheology of oceanic lithosphere. Geophys. J. Int. 142, 855-875.

Watts, A., Zhong, S., Hunter, J., 2013. The behavior of the lithosphere on seismic to geologic timescales. Annu Rev Earth Pl Sc 41, 443-468.

Zattin, M., Andreucci, B., de Toffoli, B., Grigo, D., Tsikalas, F., 2016. Thermochronological constraints to late Cenozoic exhumation of the Barents Sea Shelf. Mar Petrol Geol 73, 97-104.